Giving gully detection a HAND : Testing the scalability and transferability of a semi-automated object-orientated approach to map permanent gullies

Olivier, G., Van De Wiel, M., Castillo, C., Vallejo Orti, M. & de Clercq, W

Original citation:
Olivier, G, Van De Wiel, M, Castillo, C, Vallejo Orti, M & de Clercq, W 2024, 'Giving gully detection a HAND : Testing the scalability and transferability of a semi-automated object-orientated approach to map permanent gullies', Catena, vol. 236, 107706. https://doi.org/10.1016/j.catena.2023.107706

DOI 10.1016/j.catena.2023.107706
ISSN 0341-8162
ESSN 1872-6887

Publisher: Elsevier

Catena 236 (2024) 107706

Contents lists available at ScienceDirect

Catena

journal homepage: www.elsevier.com/locate/catena

Giving gully detection a HAND – Testing the scalability and transferability of a semi-automated object-orientated approach to map permanent gullies

George Olivier [a,b,c,*], Marco J. Van De Wiel [a,d], Carlos Castillo [e], Miguel Vallejo Orti [f,g], Willem P. de Clercq [b]

[a] Centre for Agroecology, Water and Resilience, Coventry University, Priory Street, Coventry CV1 5LW, UK
[b] Stellenbosch University Water Institute, Stellenbosch University, Private Bag X1, Matieland, Stellenbosch 7602, South Africa
[c] Department of Earth Sciences, Stellenbosch University, Private Bag X1, Matieland, Stellenbosch 7602, South Africa
[d] College of Agriculture and Environmental Sciences, UNISA, Florida 1709, South Africa
[e] University of Córdoba, Campus de Rabanales, Department of Rural Engineering, Civil Constructions and Project Engineering, Leonardo da Vinci Building, 14071 Córdoba, Spain
[f] Department of Land and Spatial Sciences, Namibia University of Science and Technology, 13 Jackson Kaujeua Street, Windhoek 13388, Namibia
[g] Institute of Geography, Heidelberg University, Im Neuenheimer Feld 348, 69120 Heidelberg, Germany

ARTICLE INFO

Keywords:
Gully erosion
Automated mapping
Gully morphology
DEM
GIS
Object-based image analysis
Height above nearest drainage

ABSTRACT

Gully erosion can incur on- and off-site impacts with severe environmental and socio-economic consequences. Semi-automated mapping provides a means to map gullies systematically and without bias, providing information on their location and extent. If used temporally, semi-automated mapping can be used to quantify soil loss and identify soil loss source areas. The information can be used to identify mitigation strategies and test the efficacy thereof. We develop, describe, and test a novel semi-automated mapping workflow, gHAND, based on the distinct topographic landform features of a gully to enhance transferability to different climatic regions. Firstly, topographic heights of a Digital Elevation Model are normalised with reference to the gully channel thalweg to extract gully floor elements, and secondly, slope are calculated along the direction of flow to determine gully wall elements. As the gHAND workflow eliminates the need to define kernel thresholds that are sensitive towards gully size, it is more scalable than kernel-based methods. The workflow is rigorously tested at different gully geomorphic scales, in contrasting geo-environments, and compared to benchmark methods explicitly developed for region-specific gullies. Performance is similar to benchmark methods (variance between 1.4 % and 14.8 %). Regarding scalability, gHAND produced under- and over-estimation errors below 30.6 % and 16.1 % for gullies with planimetric areas varying between 1421.6 m^2 and 355403.7 m^2, without editing the workflow. Although the gHAND workflow has limitations, most markedly the requirement of manually digitising gully headcuts, it shows potential to be further developed to reliably map gullies of small- to large-scales in different geo-environments.

1. Introduction

Gully erosion is a form of channelised water erosion associated with the severe degradation of land and water resources (Wen et al., 2021; Wilkinson et al., 2015). Despite gully erosion occurring in many parts of the world, in all climate zones (except polar) (Castillo and Gómez, 2016), there remains a lack of large-scale datasets regarding gully location and extent (Vanmaercke et al., 2021). Such datasets alone will help to identify areas where mitigation and rehabilitation measures are imperative. However, these datasets will be even more useful on a temporal scale as further insight can be gained on how control factors impact gully erosion morphology, dynamics, and rates, in addition to the efficacy of conservation measures.

Due to time and labour constraints, traditional methods delineating gully extents in the field (Perroy et al., 2010) or from remote imagery interpretation (Osumgborogwu et al., 2022) seldomly extend to large geographic extents. In cases where large-scale gully inventories were captured, they usually remain a snapshot in time with no subsequent coverage (e.g., Mararakanye and Le Roux, 2012).

Recently, due to technological advancements, (semi-)automated

* Corresponding author at: Centre for Agroecology, Water and Resilience, Coventry University, Priory Street, Coventry CV1 5LW, UK.
E-mail address: olivierg@sun.ac.za (G. Olivier).

https://doi.org/10.1016/j.catena.2023.107706
Received 22 June 2023; Received in revised form 27 October 2023; Accepted 21 November 2023
Available online 15 December 2023

methods mapping gullies have been proposed (Table 1). Although different (semi-)automated methodologies exist, *viz.*, traditional pixel-based (including statistical), object-orientated, and machine learning, the fundamental input data used to extract gully perimeters consist of spectral properties (d'Oleire-Oltmanns et al., 2014; Phinzi et al., 2021), Digital Elevation Models (DEM) (Chen et al., 2023; Brecheisen and Richter, 2021; Walker et al., 2020), or a combination of the aforementioned (Bokaei et al., 2023; Codru et al., 2023).

In terms of data inputs, DEMs are ideally suited because they can be used to discern distinct gully landform elements. Gullies are generally persistent elongated features consisting of locally low-positioned flat floors enclosed by short and sharp sloped sidewalls (Castillo et al., 2014; Thwaites et al., 2022). These local terrain differences are typically exploited by predetermined search window sizes (Table 1). Examples of the predetermined window sizes include Evans and Lindsay (2010) using an edge detection method, passing a mean filter subtracted from the DEM, to map gully sidewalls, where the area between the edges was then interpolated; Johansen et al. (2012) employed a min/max brightness filter to detect gully edges as the initial step in mapping gullies in their study area; Castillo et al. (2014) calculated a z-score normalisation statistic to identify gully floor and wall elements separately before joining and refining the classification; Korzeniowska et al. (2018) and Francipane et al. (2020), using a roughness index, and Walker et al. (2020), calculating elevation percentiles for various DEM derivatives.

Exploiting local terrain differences in a DEM to (semi-)automatically map gullies provides reliable results (Table 1) and should be transferable since it is based on extracting the typical gully morphology. However, determining the optimal window size remains challenging irrespective of the statistic or terrain derivative calculated for input. Evans and Lindsay (2010) suggested that the window size needs to be a function of the gully width under investigation. Under-estimating window sizes will likely result in noise, hindering detection, while over-estimating will conceal edge effects (Evans and Lindsay, 2010). Window sizes are thus sensitive to scale and are likely not able to detect gullies of varying geomorphic scales if used unedited.

Aerial and satellite imagery inputs can overcome scalability issues of DEM approaches, as probing reflectance values to (semi-)automatically map gullies do not require predefined windows (Liu et al., 2022; Mararakanye and Nethengwe, 2012). Reliable results have been obtained (Table 1) and should be scalable. However, the (semi-)automated mapping of gullies remains challenging due to the different spectral responses constituted by bare soil (wet and dry), vegetation, and possibly water, all of which can be found within the confines of gullies (Taruvinga, 2008). Phinzi et al. (2021) and Vrieling et al. (2007) also found significant differences in gully detection accuracy considering images from different seasons. These findings indicate that the transferability of unedited (semi-)automated methods using spectral reflectance remains doubtful.

Height Above Nearest Drainage (HAND) is a terrain derivative that normalises elevation in a DEM according to drainage, providing local flow path heights to the nearest stream (Nobre et al., 2011). The local height of a pixel is a permanent property reflecting drainage potential

Table 1
Recently proposed methods to map gully erosion (semi-)automatically.

Author	Method	Fundamental inputs†	DEM search window used	Average accuracy‡
Vrieling et al., 2007	Traditional pixel	Satellite imagery (15 m–30 m; visible and shortwave infrared)	–	Over prediction: 28.0 %; Under prediction: 43.2 % (*)
Evans and Lindsay, 2010	Traditional pixel	DEM (2 m)	Yes	Width error: 2.39 m
Shruthi et al., 2011	Object based	DEM (0.5 m), satellite imagery (1 m–4 m; visible and near infra-red)	No	Over prediction 0.9 % (calculated from total areas only: reference vs predicted)
Mararakanye and Nethengwe, 2012	Object based	Satellite imagery (10 m; visible)	–	Over prediction: 56 %; Under prediction: 2.4 % (*)
Castillo et al., 2014	Traditional pixel	DEM (various)	Yes	Total error (over + under prediction): 17.2 %
d'Oleire-Oltmanns et al., 2014	Object orientated	Satellite imagery (0.6 m; visible)	–	Over prediction: 16.0 %; Under prediction: 38.0 % (*)
Korzeniowska et al., 2018	Traditional pixel	DEM (1 m)	Yes	Over prediction: 32.2 %; Under prediction:22.8 % (*)
Rijal et al., 2018	Traditional pixel	DEM (1 m)	Yes	Over prediction: 14.0 %; Under prediction: 17.0 % (*)
Vallejo-Orti et al., 2019	Traditional pixel	DEM (12 m)	Yes	Over prediction: 66.1 %; Under prediction: 33.8 % (*)
Francipane et al., 2020	Object based	DEM (1 m)	Yes	Over prediction:?; Under preditction 7 % (for the training area; no statistics for the test area)
Phinzi et al., 2020	Machine learning	Satellite imagery (1.5 m–5.5 m)	–	Over prediction: 35.2 %; Under prediction: 15.7 % (*)
Utsumi et al., 2020	Object based	DEM (30 m); satellite imagery (5 m)	No	Over prediction: 20.0 %; Under prediction: 46.2 % (*)
Walker et al., 2020	Traditional pixel	DEM (1 m)	Yes	–
Brecheisen and Richter, 2021	Traditional pixel	DEM (1 m)	Yes	Over prediction: 6.8 %; Under prediction: 17.7 % (*)
Phinzi et al., 2021	Machine learning	Satellite imagery (3 m; visible and near infrared)	–	Over prediction: 39.3 %; Under prediction: 14.9 % (*)
Bokaei et al., 2023	Machine learning	DEM (?); aerial imagery (0.05 m)	Yes	Over prediction: 6.3 %; Under prediction: 31.4 % (*)
Liu et al., 2022	Machine learning	Aerial and satellite imagery (0.07 m–0.5 m)	–	Area under receiver operator curve: 0.6; overall accuracy: 84.8 %
Chen et al., 2023	Machine learning	DEM (0.5 m)	Yes	Overall accuracy: 89.8 %
Codru et al., 2023	Traditional pixel	DEM (5 m); satellite imagery (10 m; visible and near infrared)	No	Over prediction:?; Under prediction: 5 %

† DEM type (surface or terrain) and process means (e.g., LiDAR, stereo-pairs, interpolated from surveyed GPS positions, etc.) not listed.
‡ Accuracy converted to over and under prediction where possible (gully specific user accuracy was inversed to calculate over prediction; gully specific producer accuracy was inversed to calculate under prediction); converted accuracy measured by asterisk (*) next to the accuracy.

and can thus be used as a standardised framework to compare hydrological properties in different geo-environmental settings (Rennó et al., 2008). Thus far, HAND has been primarily implemented in flood inundation (Garousi-Nejad et al., 2019; Johnson et al., 2019; Liu et al., 2016) and groundwater (Miguez-Macho et al., 2020) research. Including HAND as an input for (semi-)automated methods could provide a technique that extracts gullies from a normalised DEM, which is based on its morphology (transferable) and standardised hydrological properties that do not require window sizes (scalable). Since HAND creates a normalised DEM, from which gullies would be extracted according to standardised properties, it also enhances the possibility of creating a procedure that can detect gullies in different geo-environmental settings and at geomorphic scales without the need for editing, increasing practicality.

We, therefore, aim to 1) develop a low data-intensive, repeatable, scalable, semi-automated methodology, *viz.* the Gully HAND (gHAND) workflow, to map permanent gullies, using the HAND model as the primary derivative (which, to the authors' knowledge, has not been used in gully detection strategies); 2) test the scalability of gHAND by mapping gullies of different geomorphic scales in South Africa (SA) using a 2 m DEM (GeoSmart Space Pty (Ltd), 2020) developed from aerial imagery; 3) test the transferability potential by applying gHAND at sites exhibiting different geo-environmental conditions and where different DEM products are available; and 4) compare against benchmark semi-automated mapping methods.

2. Study area

2.1. Regional setting of sites used for development and scalability testing

The Tsitsa catchment in SA was selected for the initial development and scalability testing of gHAND due to extensive gully erosion occurrence within the catchment (see Fig. 1 for location, Table 2 for the descriptors variables, and Fig. 2 for the aerial extent of the eight selected gullies). All the gullies exhibit a dendritic planform, except for one small-scale linear gully$_{(1)}$ (Fig. 2b; subindex denotes gully identifiers as per Table 2). Gully dimensions in terms of length along the main channel, maximum width, and planimetric area vary by a factor of 50.

The Tsitsa River is approximately 200 km long (Le Roux, 2018), with its confluence in steep topography into the Mzimvubu River. Upstream of the confluence, undulating plains are found, whereafter, the catchment becomes steeper again as the river approaches the Drakensberg. The aerial extent of the Tsitsa catchment is approximately 4927 km^2, located between 30°46′51″S and 31°29′15″S latitude and 27°56′13″E and 29°13′43″E longitude (Fig. 1a). The climate is sub-humid, with the mean annual rainfall ranging between 625 mm in the lower plains and increasing to 1327 mm in the mountainous upper catchment (Le Roux, 2018). The natural vegetation is predominantly from the Grasslands biome region. However, the Savanna biome is also present in the southwestern catchment (Mucina and Rutherford, 2006), where thorny acacia trees have encroached on the grassland area. The main land use in the catchment is communal grazing, with smaller pockets of commercial maize and plantations. Relicts of past water and soil conservation measures of previous commercial crop farming is present in the communal grazing areas. The geology is primarily of sedimentary strata, with large parts of the catchments underlaid by the Tarkastad and Adelaide subgroups of the Beaufort formation and Elliot group (Burger, 2013). The aforementioned sedimentary strata have been linked to derive duplex soils (soils that exhibit a strong texture contrast between surface soil and subsurface soil, mostly from translocation of clay; see Fey, 2010) with high dispersion, closely linked to high erosion susceptibility (Laker, 2004).

2.2. Regional setting of sites used to test transferability

Five gully sites were selected to test the transferability of gHAND (see Fig. 1 for location, Table 2 for the descriptors variables, and Fig. 3 for the aerial extent of the five selected gullies). Site selection was made according to data availability, whether the site exhibited a contrasting climate compared to the Tsitsa catchment, and preferably where gully detection approaches based on topographical attributes were applied previously.

A continuous gully was selected in Córdoba, Spain (Fig. 3a; the same gully as Castillo et al., 2014). The region has a Mediterranean climate, and the topography consists of rolling hills. The gully is located along the main drainage line of adjoining crop fields, exhibiting a dendritic shape (length along the main channel is 662 m; maximum width is 20.6 m, and the planimetric area is 14067.5 m^2).

In Australia, a continuous gully was selected in the Herbert catchment near Innot Springs (Fig. 3b; the gully is in the Great Barrier Reef catchment, approximately 400 km from one of the sites Walker et al., 2020 conducted a semi-automated detection approach). The area has a subtropical monsoon climate with strong seasonal rainfall patterns (Bartley et al., 2003). The gully is located on native pasture (estimated from Bartley et al., 2003) and is linear with a singular headcut (the main channel length is 202.7 m; the maximum width is 12.9 m; and the

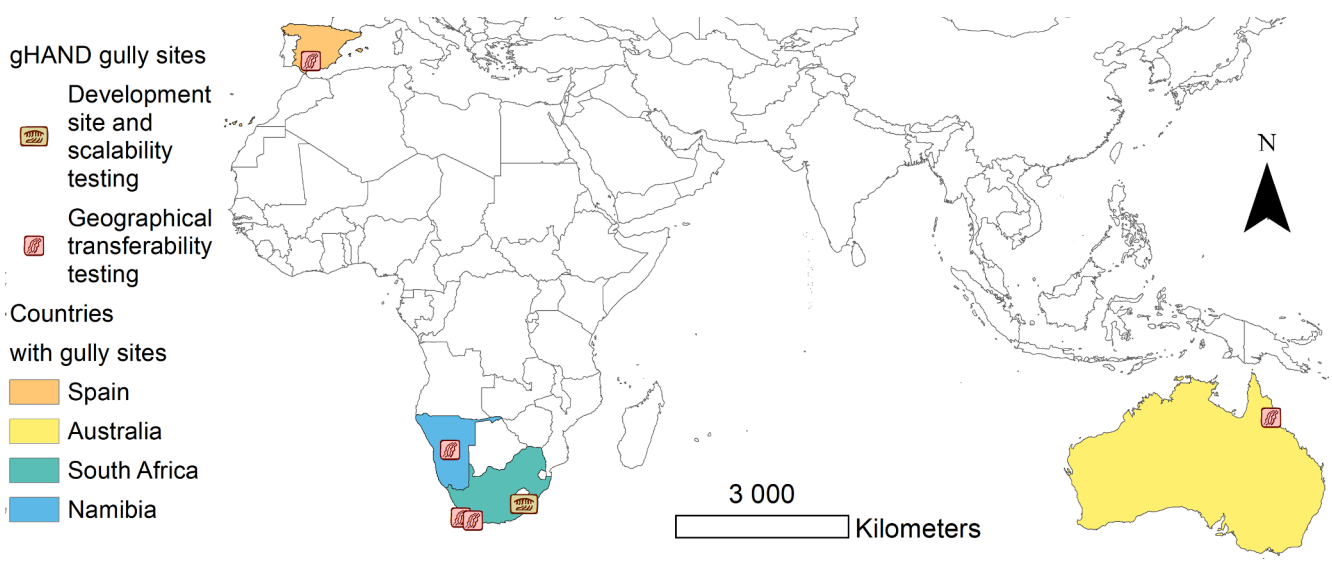

Fig. 1. Location of the sites testing the scalability and transferability of the Gully HAND detection workflow.

Table 2
Gully characteristics at sites where gully HAND was developed and tested in terms of scalability and transferability.

Site	Coordinates		Climate (according to Köppen Geiger climate classification)	Land use	Scale†	Local slope (in %)	Length of main channel (in m)	Maximum width (in m)	Planimetric area (in m^2)	Mitigation strategies
	x	y								
Development and testing scalability										
Tistsa catchment, South Africa	28.474	−31.194	Cwb (Subtropical highland)	Communal grazing	$Small_{(1)}$	9.0	183.3	18.6	1619.0	–
Tistsa catchment, South Africa	28.638	−31.105	Cwb (Subtropical highland)	Communal grazing	$Small_{(2)}$	10.2	121.3	10.6	1421.6	–
Tsitsa catchment, South Africa	28.467	−31.191	Cwb (Subtropical highland)	Communal grazing	$Medium_{(1)}$	8.1	430.9	34.3	12135.6	–
Tistsa catchment, South Africa	28.613	−31.074	Cwb (Subtropical highland)	Communal grazing	$Medium_{(2)}$	5.6	241.9	25.5	4827.1	Contour banks (on abandoned agricultural fields)
Tsitsa catchment, South Africa	28.788	−31.202	Cfb (Oceanic and Subtropical highland)	Communal grazing	$Large_{(1)}$	3.2	2142.8	39.4	70246.7	Contour banks (on abandoned agricultural fields); dam at headcut
Tistsa catchment, South Africa	28.821	−31.169	Cfb (Oceanic and Subtropical highland)	Communal grazing	$Large_{(2)}$	4.2	1881.5	37.2	38042.3	Contour banks (on abandoned agricultural fields); dam at headcut
Tistsa catchment, South Africa	28.637	−31.129	Cwb (Subtropical highland)	Communal grazing	$Colossus_{(1)}$	4.2	3236.7	121.3	355403.7	Contour banks (on abandoned agricultural fields)
Tsitsa catchment, South Africa	28.664	−31.238	Cwb (Subtropical highland)	Communal grazing	$Colossus_{(2)}$	2.9	5113.2	208.9	425403.7	Contour banks (on abandoned agricultural fields); dam at headcut
Testing transferability to other sites, including the use of different DEMs										
Herbert catchment, Australia	145.184	−17.721	Cwa (Subtropical monsoon)	Commercial grazing	Small	3.7	202.7	12.9	1530.1	–
Cordoba, Spain	−4.604	37.837	Csa (Hot summer Mediterranean)	Commercial crops	Medium	7.2	662.0	20.6	14067.5	
Swartland, South Africa	18.759	−33.278	Csa (Hot summer Mediterranean)	Commercial crops	Medium	6.0	1285.0	20.9	23246.8	Contour banks
Montagu, South Africa	20.626	−33.730	Bsk (Cool semi arid)	Conservation	Medium	1.4	134.7	20.7	2008.0	Gabions at headcuts inlcuding failed gabions in proximity to headcuts
Krumhuk, Namibia	17.096	−22.734	Bsh (Hot semi-arid)	Commercial grazing	Large	1.6	698.3	152.0	66019.3	–

† Gully scales are defined in terms of its planimetric area and thresholds were set as follow: small-scale < 2500 m^2; medium-scale 2500 m^2–25,000 m^2; large scale 25,000 m^2–250,000 m^2; and colossus scale > 250,000 m^2. Gullies are ordered according to scale, and thereafter its longitude.

planimetric area is 1530.1 m^2).

In SA, two discontinuous gullies in contrasting regions were selected. One of these gullies is located close to Montagu, in the semi-arid Karoo, with a mean annual rainfall of 231 mm (Schulze et al., 2006) (Fig. 3c; in proximity to the gully of Olivier et al., 2022). The topography is nearly flat, and the current land use is conservation-orientated with free-roaming game. The gully is classified as frontal, as the head scarps have been significantly modified by gabions placed at the incision point, in addition to older gabions in proximity, which have failed. The main channel length is 134.7 m, the maximum width is 20.7 m, and the planimetric area is 2008.0 m^2.

The second discontinuous gully is located in southwestern SA, in the wheat-growing region of the Swartland of the Western Cape (Fig. 3d). The area has a Mediterranean climate with a mean annual rainfall of 469 mm (Schulze et al., 2006). The topography consists of rolling slopes, with most of the natural shrub (*renosterveld*) removed for crops. The dendritic gully is found along the main drainage line of adjoining fields (the main channel length is 1285.0 m; the maximum width is 20.9 m; and the planimetric area is 23246.8 m^2). Soil and water conservation works significantly impact gully morphology, resulting in an almost structured expansion as first order gully channels extend behind systematically spaced contour banks.

A continuous gully was selected at Krumhuk, Namibia (Fig. 3e; the same gully as Vallejo-Orti et al., 2019). The region is semi-arid, with the mean annual rainfall ranging from 250 mm to 350 mm. The gully is located in nearly flat topography, and commercial grazing is the main land use. The gully morphology exhibits extensive lateral erosion of the sidewalls in the form of rills and smaller gullies, lowering the slope of the historically sharp-sloped gully walls and resulting in the loss of the distinct original gully channel morphology. The channel widths extend up to 152 m wide (Vallejo-Orti et al., 2019), with the landscape seemingly transitioning to a badlands landform.

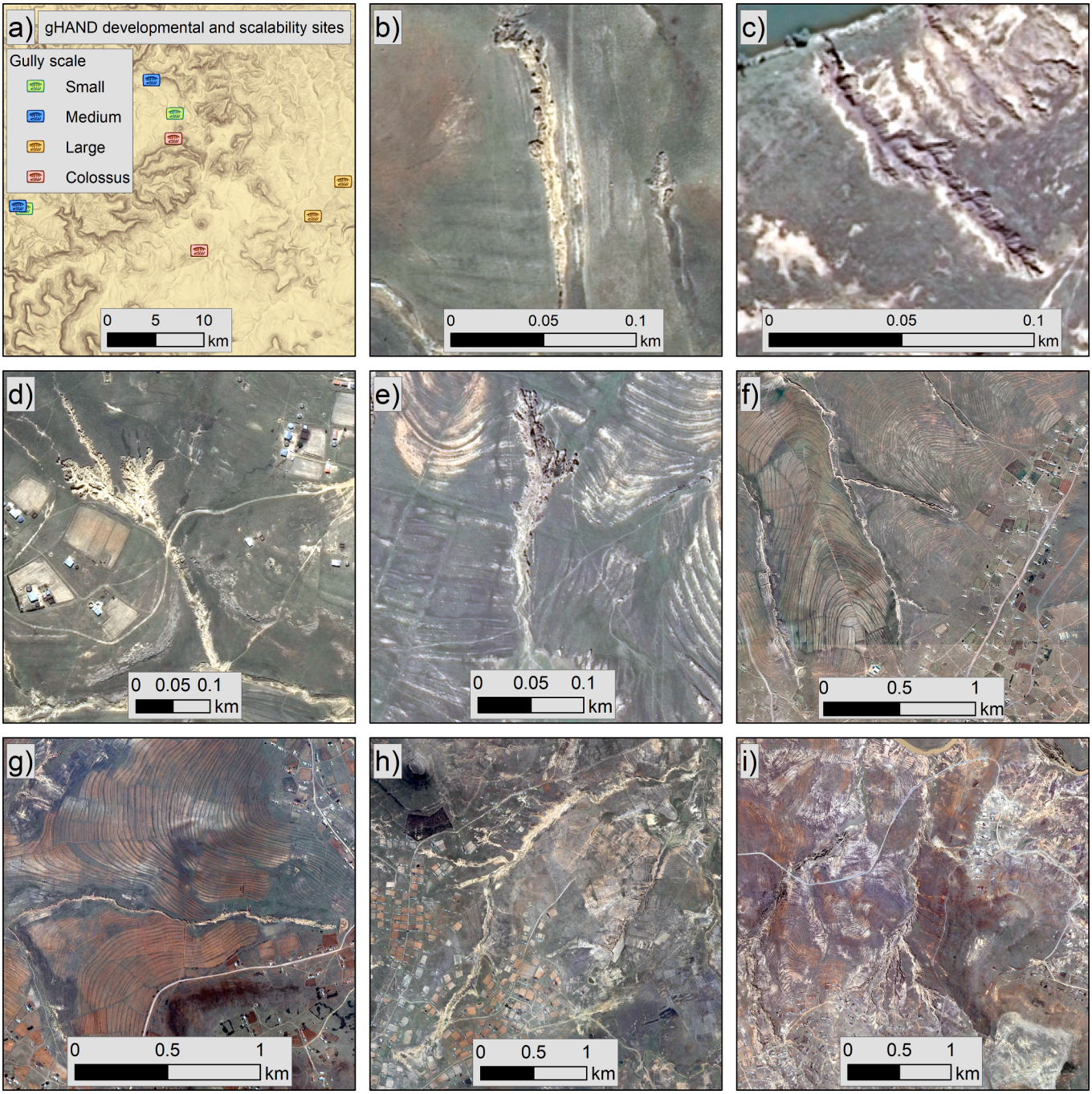

Fig. 2. Gully sites in the Tsitsa catchment, South Africa, which were used to develop and evaluate the scalability of the Gully HAND workflow: a) location of the eight gully sites overlaying a slope raster; b and c) small-scale gullies;); d and e) medium-scale gullies; f and g) large-scale gullies; h and i) colossus-scale gullies (aerial imagery was retrieved from the Department of Rural Development and Landform, available at http://www.cdngiportal.co.za/cdngiportal/).

3. Materials and methods

3.1. Datasets

In SA, GeoSmart Space Pty (Ltd) (2020) created a 2 m national DEM (known as DEMSA2) from aerial imagery (spatial resolution of 0.5 m), augmented by SRTM data in flatter terrain, covering approximately 96 % of SA. The gHAND workflow used the 2 m DEM as input for the sites in the Tsitsa catchment and the Swartland, SA (Table 3). The same aerial imagery used in generating the 2 m DEM was used as a base map to digitise reference gully datasets manually.

In Montagu, SA, a 0.07 m DEM was created using commercial software (AgiSoft Metashape Professional 1.8.1 (Agisoft LLC, St. Petersburg, Russia)). Imagery captured from a DJI Mavic 3 equipped with a 4/3 CMOS Hasselblad camera was used as input for creating the DEM. A reference dataset was digitised from the same imagery used as input into Agisoft Metashape Professional 1.8.1 (Agisoft LLC, St. Petersburg, Russia).

In Córdoba, Spain, a 0.06 m DEM was created using commercial software (Pix4D) from photogrammetric methods (see Castillo et al., 2014 for more detail). A differential Global Positioning System (dGPS) with cm accuracy was used to map the gully perimeter by the change-in-slope criterion. The dGPS points were taken in-field on the flight date and used as a reference boundary for the gully feature.

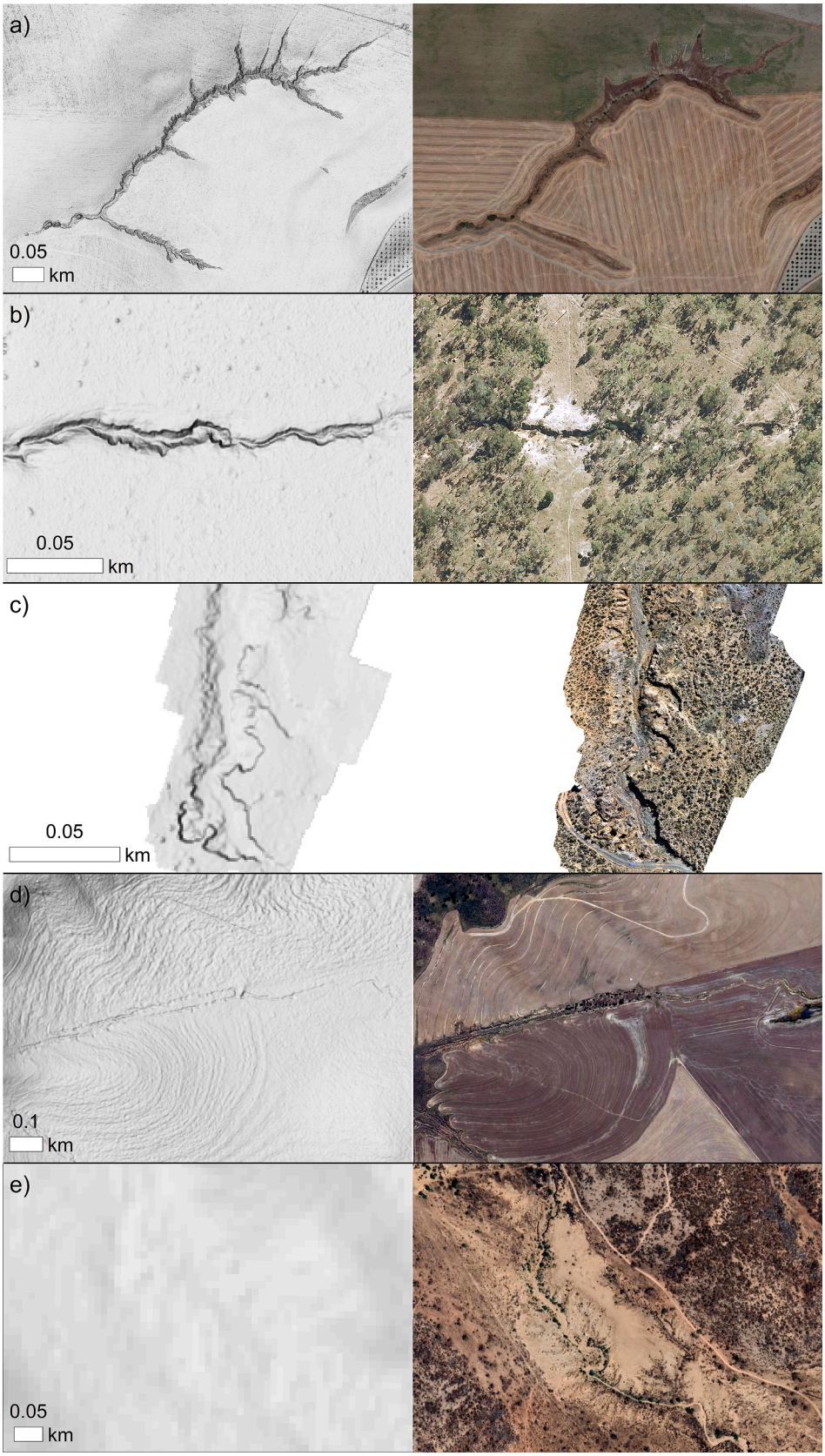

Fig. 3. A multi-directional hillshade and aerial image showing topographical detail captured in the varying DEM spatial resolutions and the aerial extent of the gully sites used to evaluate the transferability of the gully HAND workflow: a) Córdoba, Spain with an input DEM of 0.06 m (Castillo et al.,2014; satellite imagery courtesy of Google Earth (21/7/2018)); b) Herbert catchment, Australia with an input DEM of 0.5 m (Geoscience Australia National Elevation Data Framework, available at http://www.ga.gov.au/elvis/); c) Montagu, South Africa with an input DEM of 0.7 m; d) Swartland, South Africa with an input DEM of 2 m (GeoSmart Space Pty

(Ltd), 2020, aerial image retrieved from the Department of Rural Development and Land Reform, available at http://www.cdngiportal.co.za/cdngiportal/); e) Krumhuk, Namibia with an input DEM of 12 m DEM (Vallejo-Orti et al., 2019; satellite imagery courtesy of Google Earth (23/10/2021)).

Table 3
DEM data for all sites.

Site	Source	Parent data from which the DEM is derived	DEM type	Spatial resolution	Vertical accuracy	Horizontal accuracy	Semi-automated detection method
Córdoba, Spain	Castillo et al., 2014 implemented commercial software Pix4D	Aerial imagery	Surface	0.06 m	0.23 m	0.09 m	NorToM (Castillo et al., 2014) and gHAND
Herbert catchment, Australia	LiDAR collected for Reef Trust, by Atlass Aerometrex, with CSIRO as the project manager	LiDAR	Terrain	0.5 m	0.2 m	0.8 m	gHAND
Montagu, South Africa	By Author	UAV aerial	Surface	0.7	N/A	N/A	gHAND
South Africa (all sites, except Montagu)	GeoSmart Pty (Ltd)	Primarily aerial imagery	Surface	2 m	0.5 m	1 m	gHAND
Krumhuk, Namibia	DLR (German Aerospace Center)	Satellite imagery	Surface	12 m	2 m	10 m	IMR, SMPF, and MPCA (Vallejo-Orti et al., 2019) and gHAND

In the Herbert catchment, Australia, arial flights from 2018 were flown to collect LiDAR data with a target density of 16 points per square meter (Geoscience Australia National Elevation Data Framework, available at https://www.ga.gov.au/elvis/). Aerial imagery from the same flight, supported by a multi-directional hillshade, was used to digitise a reference dataset manually.

In Krumhuk, Namibia, a 12 m TanDEM-X was acquired from a TerraSAR-X DLR mission in January 2015 (see Vallejo-Orti et al., 2019 for further details). A reference dataset was initially derived in the field with a Global Navigation Satellite System in 2018. The reference dataset was subsequently refined using 0.5 m Pleiades imagery captured in December 2016 to reduce potential errors due to the temporal variance between the DEM and reference datasets (Vallejo-Orti et al., 2019).

3.2. gHAND procedure

The gHAND workflow is based on two detection variables, viz., HAND and slope. The first step to derive HAND requires a conditioned DEM to extract drainage pathways. The HAND method developed by Rennó et al. (2008) uses a breaching method like the one from O'Callaghan and Mark (1984) to eliminate sinks. Once sinks are removed, the D8 flow approach (O'Callaghan and Mark, 1984) is applied to identify Local Drain Directions (LDD). The D8 flow approach is deemed suitable as lateral movement along a flat plane would have little impact on the final HAND pixel value (Nobre et al., 2011). The drainage pathways are established by defining contributing area and geomorphic curvature thresholds to identify the river headwater (Rennó et al., 2008).

The initial steps to calculate gully drainages following gHAND is similar to HAND. Input DEMs are hydrologically corrected in ArcGIS 10.6.1 (Environmental Systems Research Institute (ESRI), Inc., Redlands, CA, USA) using the depression filling method from Planchon and Darboux (2002). Subsequently, LDD is acquired from the D8 flow approach. The upstream drainage areas of gullies vary significantly according to local environmental factors (Poesen et al., 2003; Vanmaercke et al., 2021); therefore, using a singular contributing threshold to determine gully headcuts was assumed invalid. Instead, a rapid approach to map gully headcuts as point features from aerial photos, enhanced with a multi-directional hillshade, is followed. Gully drainage pathways are defined using the digitised points as a weighted input.

Once drainage pathways are established, the second step is normalising the DEM according to its derived drainage pathway (Fig. 4). A drainage connectivity raster is calculated by grouping all pixels to its nearest local drainage point. HAND is calculated for each pixel by subtracting its elevation value from its grouped outlet point (Nobre et al., 2011). Drainage pathways will, therefore, be zeroed as they are subtracted from themselves, implying a flat topographic reference without any gravitational drainage potential (Rennó et al., 2008). Pixels that are adjacent to the drainage pathway and on the hillslope will yield a value associated with the vertical height to its nearest drainage pathway.

Subsequently, gHAND uses a (Geographic Object-Based Image Analysis) GEOBIA segmentation approach to identify gully floor and wall elements from HAND and slope values. Due to topographical gully floor oscillations, gully floor elements are expected to have near-zero HAND values. Gully wall elements are identified by steep slopes along the flow path and further constrained by HAND. GEOBIA segmentation was selected as it has outperformed exclusive pixel-based approaches in extracting gully features because of the ability of the object-orientated approach to extract data regarding shape, proximity, and neighbouring relationships (Francipane et al., 2020). The multi-resolution segmentation process creates objects from a bottom-up approach that groups pixels according to the relative homogeneity within the input variables (Blascke, et al., 2014).

The scale parameter controls the allowable variance of homogeneity and is based on a combination of shape and colour properties (in our case, the HAND and slope values) and compactness (how closely related the shape is to a circle) (Trimble Germany GmbH, 2023). Due to gullies mostly exhibiting linear morphologies, emphasis was placed on shape (0.8), and compactness was reduced to 0.4. Larger scale parameters yield larger objects and *vice versa* (Karydas and Jiang, 2020). Gullies are predominantly linear, following drainage lines, although exceptions such as alluvial amphitheatre gullies also exist (Shellberg and Brooks, 2012; Thwaites et al., 2022). Therefore, a smaller scale parameter was desirable, given the 2 m DEM resolution. A trial-and-error calibration was conducted on a medium-scale gully, whereafter a scale parameter of 4 was selected (see supplementary material, Table A1, which showed larger objects resulting in higher over-estimation errors). To allow the scale factor to transition with changing spatial resolution, we employed a simple division process:

$$Sf^{\sim} = \frac{Sf}{S_{res}} \tag{1}$$

where Sf is the original scale factor of four, established for the 2 m DEM, S_{res} is the spatial resolution of the new input DEM, and $Sf^{\sim}$ is the calculated scale factor to be used during multi-resolution segmentation for the given DEM. However, a minimum scale factor of 2 was used for coarser spatial resolutions.

The complete gHAND workflow and associated threshold settings are described in Table 4. Parameter sensitivity analysis was conducted

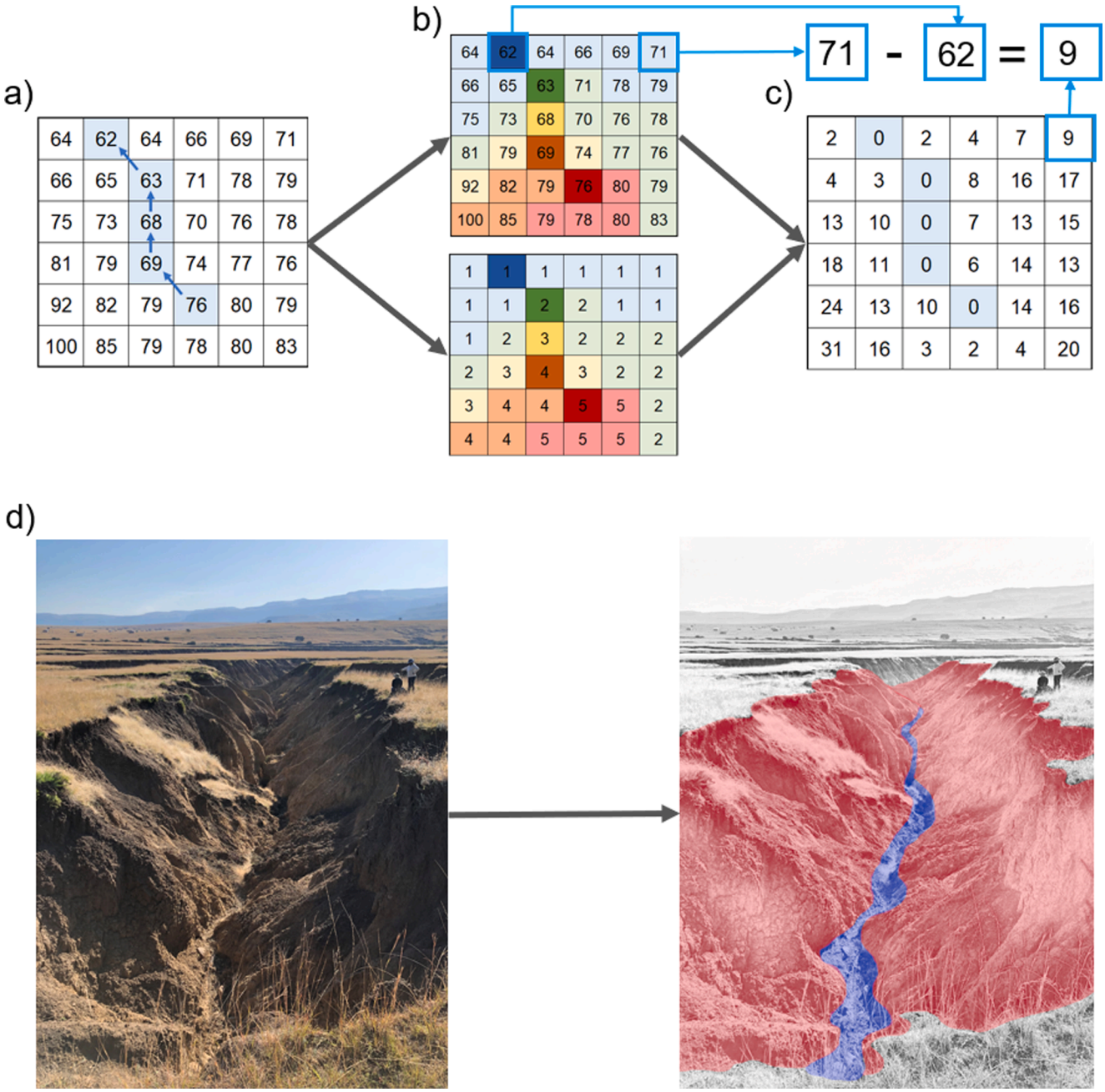

Fig. 4. Normalising the DEM according to Height Above Nearest Drainage (HAND) to highlight the distinct morphology of a gully channel: a) DEM values of a DEM with the flow direction coded by blue arrows; b) pixel values are grouped according to its nearest outlet; c) HAND is calculated by subtracting DEM pixel values from the height value of its nearest outlet (after Nobre et al., 2011); d) graphical illustration of how gully HAND uses HAND to identify the gully floor (in blue) and uses slope, constrained by HAND, to identify sharp sloped gully walls (in red). (For interpretation of the references to colour in this figure legend, the reader is referred to the web version of this article.)

regarding the placement of manually digitised gully headcuts (see supplementary material, Figs. A1 and A2) and DEM spatial resolution (see supplementary material, Fig. A3).

3.3. Limited threshold editing of gHAND

Although we aimed to identify a method that could be scalable and used without editing for a range of gully sizes, we decided to minimally tweak gHAND for the colossus scale gully to establish whether detection accuracy improvement could be made. Threshold changes were made based on local knowledge and shown in Table 4.

3.4. Accuracy assessment

The gHAND segmented mapping results were evaluated by measuring the dissimilarity between gHAND-derived and reference polygons (like Castillo et al., 2014) from

$$E_O = \frac{\sum |H_i - r_i|}{R_{Ai}} \tag{2}$$

$$E_U = \frac{\sum |r_i - H_i|}{R_{Ai}} \tag{3}$$

$$E_{tot} = |E_o| + |E_u| \tag{4}$$

Table 4
The gully HAND workflow and thresholds.

Process classification †	Software application	Step	Output	Description	Environment setting	Tool used
Pixel-based	ArcGIS 10.1.6	1	Conditioned DEM	Fill sinks		Fill (*Spatial analyst)*
		2	Additional flow direction and slope	Calculate the flow direction and Drop Raster slope	Dinf method; include DropRaster as output, which is the slope along the flow path	Flow direction (*Spatial analyst*)
		3	Gullied drainage	Generate a multi-directional hillshade		Open *window analysis.* Select the conditioned DEM and add the hillshade function – select multi-directional
				Digitise gully headcuts as points	Upon completion edit the ID field – Set all to 1	Editor
				Rasterise the digitised points	Set processing extent to DEM (output 1); snap raster to DEM; copy spatial resolution from DEM	Feature to Raster (*Conversion)*
				Reclassify *NoData* to zero values		Reclassify (*Spatial analyst*)
				Calculate the flow direction	D8 flow approach	Flow direction (*Spatial analyst*)
				Calculate the weighted flow accumulation	Use the rasterised gully headcuts (output 2) as weight raster input	Flow accumulation (*Spatial analyst*)
				Create a binary stream network		Reclassify (*Spatial analyst*)
		4	HAND	Calculate the height above nearest drainage	- Stream raster: Output 3 - Surface raster: Output 1- Flow direction raster: Output 2 (Dinf) - Flow distance type: Vertical- Flow direction type: Dinf	Flow distance (*Spatial analyst*)
Object-based	Ecognition Developer 9	5	Generate and classify gully elements	Create meaningful objects from homogenous pixels	Equal weighting for Drop Raster (output 4) and HAND (output 5); Scale parameter: 4, Shape factor: 0.8; Compactness factor: 0.4	Multiresolution segmentation
				Use a threshold approach to identify the gully floor	Use "*Low_HAND*" threshold at image object level	Multi-threshold segmentation
				Merge gully floor elements		Merge region
				Remove all objects containing *NoData* values	Use HAND < 0	Assign class
				Use a threshold approach to identify gully wall candidates	Use "*Heigh_HAND*" and "*Bluff_DropR*" thresholds at image object level	Multi-threshold segmentation
				Combine gully wall candidates		Merge region
				Shrink gully wall elements to off-set overprediction	One iteration	Pixel-based object resizing
				Merge gully wall candidates		Merge region
				Merge gully floor and gully wall candidates		Assign class
		6	Refining gully network	Grow the merged gully candidates	One iteration	Pixel-based object resizing
				Merge objects		Merge region
				Fill any holes found within the classification	Set the area smaller than "*Isle_Hole*" and ensure that the gap is surrounded by gully candidates (relative border = 1)	Assign class
				Merge objects		Merge region
				Smooth gully candidate objects	One iteration (shrink)	Pixel-based object resizing
				Remove any dangling phantom gully branches	Set minimum threshold "*Min_Phan*" with objects below set to unclassified	Assign class
		7	Export gully classification	Save the mapped gully		Export vector layer
Threshold settings			Standard		Colossus Edited	
			Low_HAND	0.5 m	1 m	
			High_HAND	6 m	10 m	
			Bluff_DropR	25 %	25 %	
			Isle_Hole	200 m^2	400 m^2	
			Min_Phan	200 m^2	400 m^2	

where E_o is the over-estimation representing the total area of polygon segments derived from gHAND that is outside the perimeter of the reference polygon, E_u represents the under-estimation of the gHAND mapped polygon by finding the total area of reference polygon segments that exceed the predicted gullied polygon by gHAND, E_{tot} is the combined error of E_o and E_u, H_i is the calculated area of the i-th polygon segment mapped by gHAND, r_i is the area of the i-th reference polygon segment, and R_{Ai} is the total gullied area according to the i-th reference polygon.

The HAND and slope pixel values for all errors (over- and under-predicted areas) were extracted to identify the primary building block causing gHAND mapping errors. Additionally, aerial imagery of areas of erroneous mapping was extracted to identify specific gully process, morphology, or landscape elements resulting in errors.

Besides evaluating the mapping errors in isolation, additional validation of gHAND was conducted by comparing its performance with benchmark methods, *viz.*, NorToM in Spain (Castillo et al., 2014) and IMR, SMPF, and MPCA methods in Namibia (Vallejo-Orti., 2019). These benchmark methods were explicitly developed for region-specific gullies; therefore, comparing gHAND to them provides a more comprehensive evaluation of the transferability potential of gHAND.

4. Results

4.1. Testing scalability: Gully mapping in the Tsitsa catchment, SA

Fig. 5 shows the areal errors incurred by the gHAND workflow for gullies increasing in geomorphic scales. The lowest error was recorded for medium-scale$_{(2)}$ (total error: 18.6 %), while the most significant error occurred from mapping the largest colossus-scale$_{(2)}$ gully network (total error: 52.1 %). Comparable results with a total error variance <8.4 % were obtained for the remainder of the gullies despite their planimetric area varying by two orders of magnitude. Under-estimation error is the highest contributor to total error (10.8 %–48.9 %), except for the small-scale$_{(1)}$ gully. Fig. 6 shows that the total areas predicted by gHAND are lower than the reference dataset. The lower calculated areas would assume that under-estimation is likely to be caused by gully morphology, process, and scale, and mostly not the poor extraction of drainage pathways that artificially shift the gHAND mapped gully, which would have caused similar area extents coupled with large under-estimations. Over-prediction errors are <16.1 % and are inverse to geomorphic gully scales.

Introducing local knowledge in the form of thresholds for the colossus scale gully lowered total error by 12.5 % (colossus-scale$_{(2)}$) and 14.6 % (colossus-scale$_{(1)}$), respectively. The unedited gHAND produced a total error of 22.5 % for the 355403.7 m^2 colossus-scale$_{(1)}$ gully and 37.5 % for the 425403.7 m^2 colossus-scale$_{(2)}$ gully.

4.2. Testing transferability: Gully mapping in various geo-environments

Fig. 7 shows the areal errors produced by gHAND at transferability sites, which are ordered according to the spatial resolution of the input DEM. Total error has a positive relationship with DEM spatial resolution. Comparable total errors were incurred at sites with a DEM resolution sub-1 m (20.8 %–21.8 %). At Swartland, SA, a total error of 49.8 % was incurred by gHAND using a 2 m DEM as input, while a 53.2 % total error was calculated for the 12 m DEM at Krumhuk, Namibia. Over-estimation errors are the principal contributor to total error for the sub-1 m DEMs (between 12.2 % and 14.6 % more than under-estimation). In contrast under-estimation errors were the main contributor to total error when using the 2 m and 12 m DEM as input in gHAND.

4.3. Comparison with benchmark workflows in Namibia and Spain

Fig. 8 compares the areal errors obtained from gHAND with benchmark methods developed for the site-specific gully topology at Córdoba, Spain (Castillo et al., 2014) and Krumhuk, Namibia (Vallejo-Orti et al., 2019).

At Córdoba, Spain, the mapping error incurred by gHAND is comparable with NorToM (Castillo et al., 2014) (Fig. 8a). NorToM used different kernel sizes (20 m–60 m) to map the permanent gully at Córdoba, Spain optimally. Total errors produced by NorToM ranged between 10.8 % and 23.1 %, which is kernel size dependent (mean total error of all kernel sizes = 16.5 %). The gHAND workflow incurs a total error of 20.8 %, which arises mainly due to an over-estimation error of 17.7 %.

At Krumhuk, Namibia, three methods were implemented, namely IMR, SMPF, and MPCA (Vallejo-Orti, 2019) (Fig. 8b). The inverse of the reported producer and user accuracies reported by Vallejo-Orti et al. (2019) was calculated to produce an equivalent over-estimation, under-estimation, and total mapping errors for comparison with gHAND. The MPCA method produced the lowest total error (60.2 %) of the benchmark methodologies. gHAND was comparable to the optimal benchmark method in Krumhuk, incurring a total error of 53.2 %, which mainly resulted from a significant under-estimation error of 47.9 %.

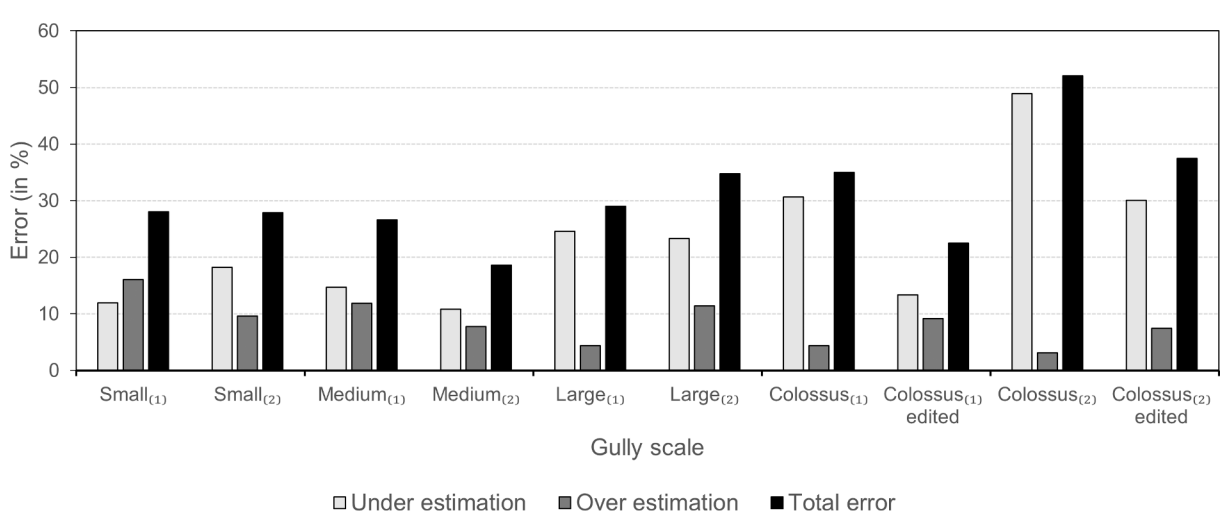

Fig. 5. Under-estimation, over-estimation, and total errors of the gully HAND workflow for gullies of increasing geomorphic sizes in the Tsitsa catchment, South Africa.

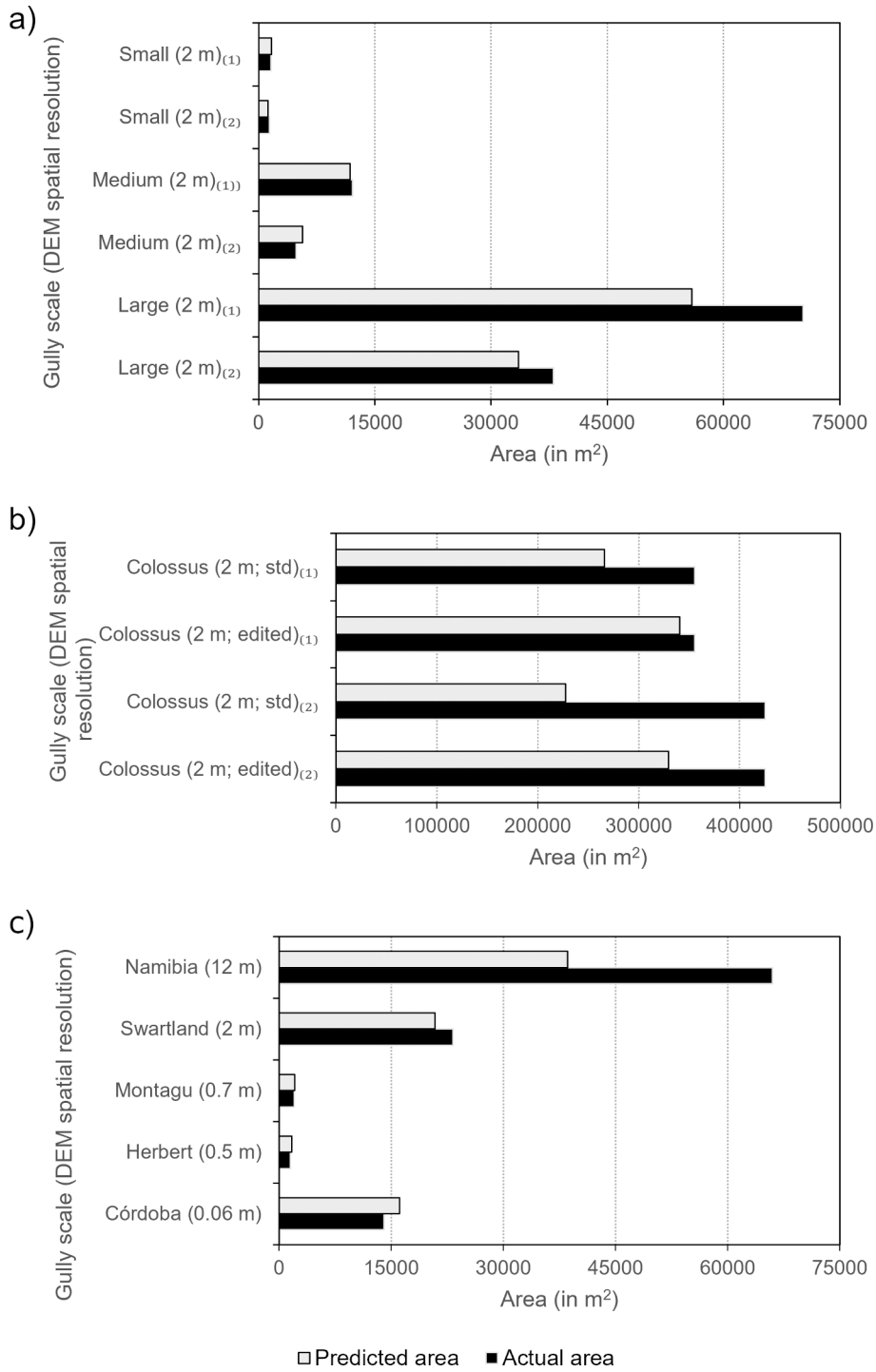

Fig. 6. A comparison of the total areas obtained from the reference dataset and the gully HAND method for all the gully sites: a) Tsitsa small-, medium-, and large-scale gullies; b) colossus-scale gully (edited and non-edited gully HAND); and c) at the transferability sites.

4.4. Impact of gully morphology and processes on gHAND accuracy

The gHAND workflow tolerated different gully shapes and channel floor oscillations (Fig. 9). The classical V- and U-shape gullies were accurately determined by gHAND, showing low errors. The gHAND workflow mapped complex gully floor topography with low errors, e.g., gully floor undulations below the 0.5 m HAND threshold (Fig. 9a) and gully floor fluctuations above the 0.5 m HAND threshold, albeit with steep-sloped undulations (Fig. 9b).

Over-estimation errors by gHAND occurred at gully walls, headcuts, and narrow interfluves (Fig. 10). More than 70 % of the over-estimated error pixels are above the 25 % slope threshold, while 12.9 % are below the 0.5 m HAND threshold (Fig. 10e). Slope commits five times more pixels to over-prediction in the gHAND model compared to HAND. The most typical error is caused by slope pixels adjacent to gully walls with pixel values above 25 % (and above the 0.5 m HAND threshold) (Fig. 10 a, b). Less frequent errors occur when the slope threshold is below 25 %. For example, in Fig. 10c, a narrow interfluve was incorrectly mapped as part of the gully, which may have been committed to over-estimation from the pixel-based growing step in gHAND (Table 4). Over-

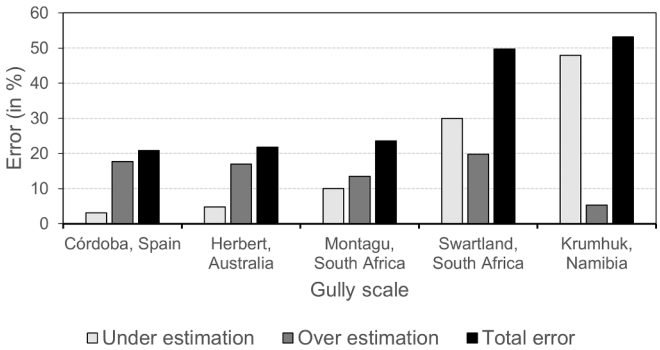

Fig. 7. Under-estimation, over-estimation, and total errors of the gully HAND workflow recorded at the transferability sites, ordered according to DEM spatial resolution.

estimation errors also occur at pixel values below the slope and HAND threshold, where incorrect drainage pathways were extracted and at shallow headcuts shallower than 0.5 m, which results in the gHAND gully polygon leaching beyond the headcut (Fig. 10d).

Like the over-estimation errors, under-estimation is also influenced by slope, but mostly due to gully walls having a lower slope than the 25 % threshold (Fig. 11e). However, significant under-estimated areas also have slope values larger than 25 % (Fig. 11a, b). In contrast, fewer than 1 % of pixels underestimated gullies with values lower than the 0.5 m HAND threshold. Examples of areas where pixels are omitted to under-estimation errors due to being below the 25 % threshold include gully floor topography, where an increase beyond 0.5 m occurs at a gradual slope, such as at a point bar (Fig. 11c). However, under-estimation can also happen in wide gully channels adjacent to the thalweg (Fig. 11d) or where subsurface flow has resulted in sagged gully banks or recently collapsed pipes (Fig. 12). Under-estimation errors occurred at frontal head scarps where overflow has resulted in deep, closely spaced flutes or multiple narrow, deep channels with tapered interfluves (Fig. 11d, Fig. 13).

5. Discussion

5.1. Advantages of gHAND

Implementing the gHAND workflow has several interrelated advantages. Firstly, it uses limited input; secondly, it does not require pre-defined search windows, making the workflow easily scalable; thirdly, it discriminates gully dimensions adequately in the presence of water and soil conservation techniques; and lastly, it uses measurements associated with gully morphology, like those measured in-field.

In terms of limited input, gHAND only requires a DEM of the study area. Moreover, we demonstrated that gHAND could be used from DEMs derived from different sources (aerial imagery, LiDAR, and satellite imagery), spatial resolutions (although there is a decrease in accuracy metrics associated with coarsening resolution) and type (surface and terrain), while performing adequately at different geomorphic scales and in geo-environmental environments.

Due to using a normalised DEM in gHAND, the requirement of using defined search windows is eliminated, thus presenting a workflow that is scale independent. Search windows are typically a crucial strategy in (semi-)automated methods using DEMs to extract distinct gully landforms from their local terrain (Table 1). Although, Castillo et al. (2014) argue that calculating z-score statistics from predefined search windows creates a scale-independent methodology, its scale dependency is evident from: 1) the array of window sizes used and 2) the acknowledgement that "landscapes with highly contrasting gully widths might require the use of several runs with different window sizes" (Castillo et al., 2014: p2013). Contrastingly, gHAND produced a total error of <=35 % for gullies with a planimetric area varying two orders of magnitude (1421.6^2 up to 355403.7 m^2) when testing scalability in the Tsitsa catchment, SA, without the need for editing the workflow. Additionally, due to the identification of gullies being strongly associated with low HAND values in proximity to the gully thalweg, gHAND is unlikely to experience detection decay in strongly sloped landscapes (as demonstrated in the strongly sloping Tsitsa catchment, SA) or where significant hillslope noise is present on high resolution DEMs (as demonstrated in Córdoba, Spain).

In terms of soil and water conservation techniques, gHAND seems primarily unaffected by their presence. Relic contour banks from abandoned cultivated fields and dams placed at headcuts had no effect on gHAND in the Tsitsa catchment, SA. Similarly, gabions that altered headcut morphology, did not adversely affect gHAND performance at gully site in Monatgu, SA. In Swartland, SA, contour banks were present on rolling hills of a grain field. Although a total error of 49.8 % was calculated, the contour banks had limited impact, only committing small over-estimations at a few headcuts that extended behind the contour bank due to its shallow depth.

Lastly, gHAND exploits gully morphology in quantitative measures to map gully elements, augmenting transferability. The gHAND workflow adequately detected V- and U-shaped gullies and was able to extract dendritic and linear gullies. An additional advantage of implementing thresholds linked to morphology is that they are associated with field measurements, enhancing practicality, unlike more obscure measurements and statistics with little physical relevance to the actual gully, especially when implementing spectral datasets (Phinzi et al., 2020, 2021; Vrieling, 2007), e.g.,

$$P(X|w_i) = \frac{1}{2\pi|V_i|^{\frac{1}{2}}} exp[-1/2(X-M_i)^T V_i^{-1}(X-M_i)] \quad (5)$$

"where X is the pixel's data vector in all spectral bands, n is the number of spectral bands, M_i is the mean vector for class w_i, and V_i is the variance-covariance matrix for class w_i" from Vrieling et al., (2007:2727).

5.2. gHAND model disadvantages and study limitations

Although implementing gHAND has several advantages, it also has limitations related to manual input, gully morphology and processes, gully area, and the use of proprietary software.

The gHAND workflow requires gully headcut locations to be manually digitised to allow accurate normalisation of the DEM according to HAND. This can introduce user bias and uncertainty. However, a sensitivity analysis showed that performance was not severely affected by the exact placement of the point to implicate the headcut (supplementary material, Fig. A1). Therefore, a rapid mapping process of gully headcuts should enable the successful application of gHAND. In some regions, gully headcut inventories exist, mapped to assess gully occurrence and density (Hayas et al., 2017; Vanderkerckhove, 1998). At such locations, gHAND can augment findings, but manual digitising is a prerequisite in a new study site. It would be beneficial to find a way to automate gully headcut identification, or alternatively identify gully headcut susceptibility zones (such as implementing the frequently used topographic threshold concept; see Rossi et al., 2022; Torri and Poesen, 2014) in which to search for gully headcuts to be mapped, to make regional mapping more feasible. Other semi-automated detection methods do not have this limitation (e.g., Castillo et al., 2014; Mararakanye and Nethengwe, 2012; Vallejo-Orti et al., 2019; Vrieling et al., 2007; Walker et al., 2020), although spectral methodologies do require gully inventory maps to be generated for training purposes (Mararakanye and Nethengwe, 2012; Phinzi et al., 2021; Taruvinga, 2008; Vrieling et al., 2007).

The degree of error of gHAND was linked to the complexity and scale of gully morphology and processes. The lowest error of gHAND occurred at Córdoba, Spain, and Herbert, Australia, where the highest spatial resolution DEMs were available but also showed low morphological

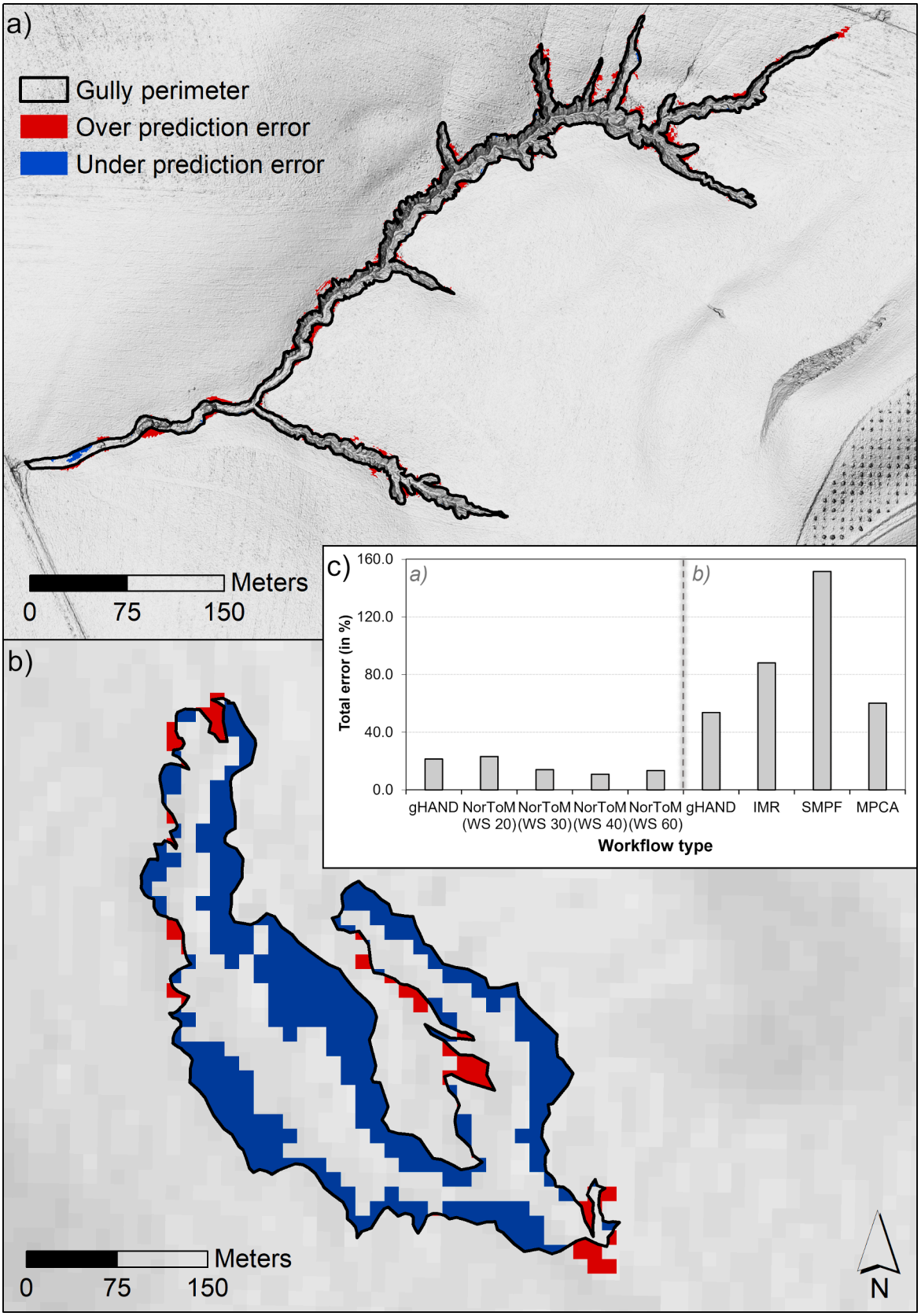

Fig. 8. Comparison of gully HAND error with benchmark methods. Over-estimation and under-estimation errors from gully HAND are superimposed onto a multi-directional hillshades from a) Córdoba, Spain, and b) Krumhuk, Namibia, with error statistics for gully HAND and the benchmark methods shown in c).

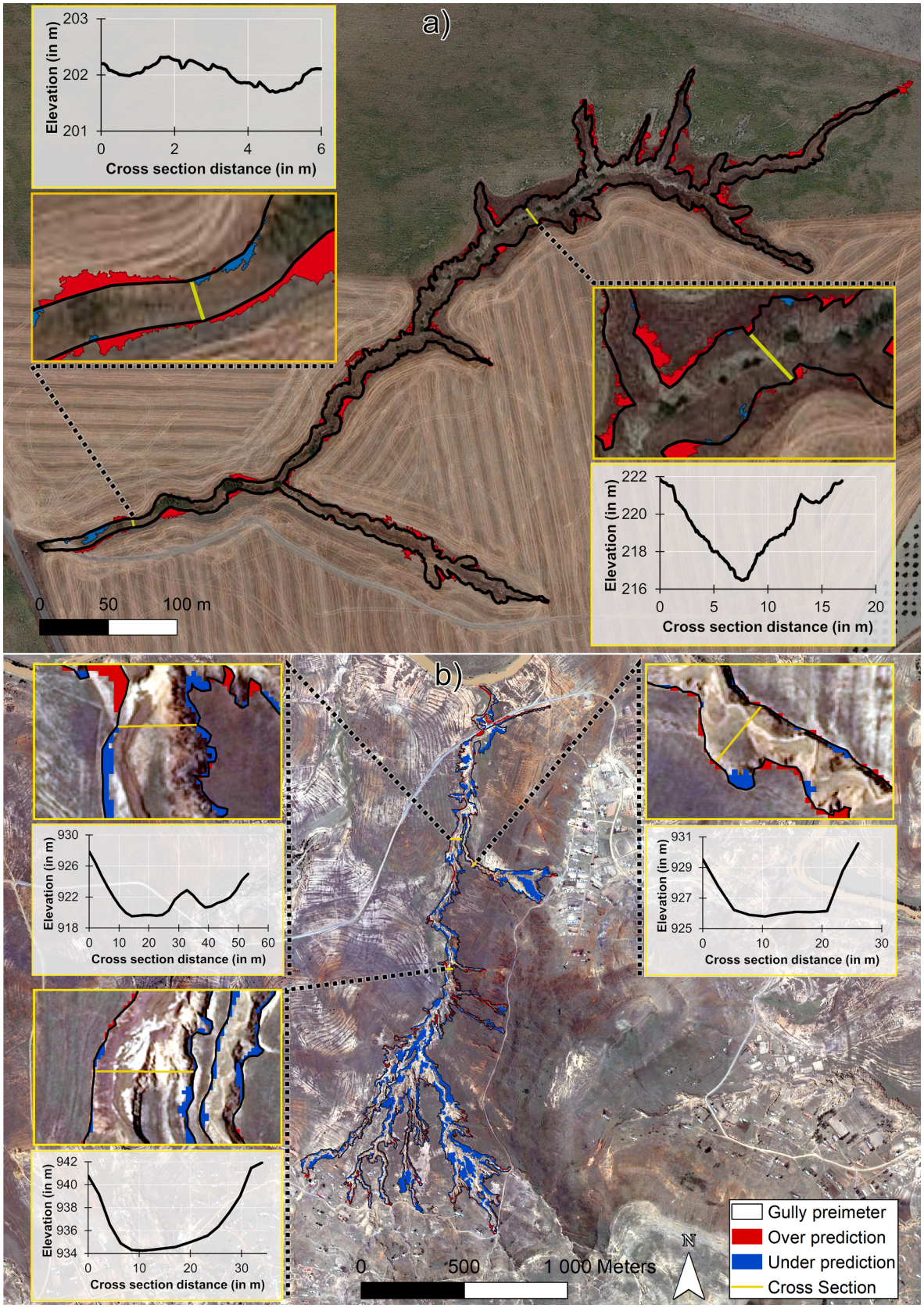

Fig. 9. The gully HAND workflow was able to accurately map various gully floor geometries and gully shapes. Examples are shown at a) Córdoba, Spain, where low errors were found in V-shaped channels upstream and complex gully floor topography downstream, where fluctuations stayed below the 0.5 m lower Height Above Nearest Drainage threshold; and b) in the Tsitsa catchment, SA, in U-shaped channels and complex channels where gully floors showed fluctuations above 0.5 m, although at a steep slope.

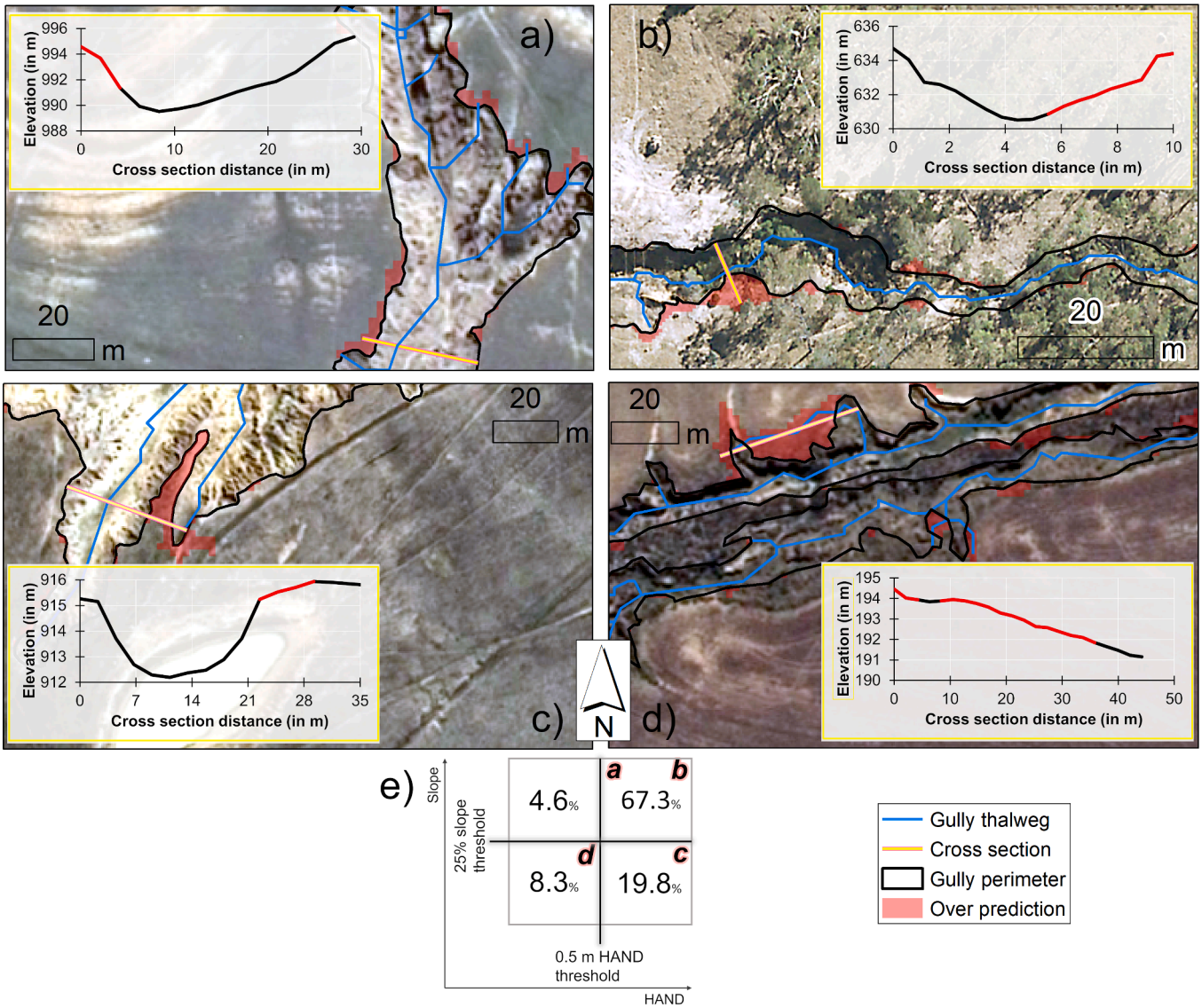

Fig. 10. Area of over-estimation error by gully HAND symbolised in red on the aerial imagery and cross sections: a and b) over-estimation pixels in proximity to gully walls with steep slopes and high Height Above Nearest Drainage (HAND) values, c) over-estimation site exhibiting slopes below the slope threshold and above the low HAND threshold; and d) over-estimation exhibiting pixels values below the slope and low HAND thresholds; e) diagram showing in which quadrant the over-estimated pixels are found (n = 574168); the location of the insert maps a, b, c, d are also located in the quadrants. (For interpretation of the references to colour in this figure legend, the reader is referred to the web version of this article.)

complexity, with clear and well-defined steep slopes. As the gully scale increased towards the colossus scale, complex gully morphology, some of which are scale-related, became evident, especially in under-estimation errors. Within the gully channel, gradual increases in height from the thalweg above 0.5 m resulted in under-estimations, which can be process- (e.g., the point bar in Fig. 11e, 12) or scale-dependent (Fig. 12). Slumping of gully walls caused by subsurface processes or newly gullied pipe collapses (Fig. 12) may yield gully slope elements below the 25 % slope threshold set in gHAND, resulting in under-estimation errors. Frontal head scarps exhibiting deep, closely spaced flutes or multiple narrow, deep channels with tapered interfluves (Fig. 11g, 13) were under-estimated. However, it was expected to be detected by gHAND due to high slope values. The reason for under-estimation is likely due to small areas of low slopes interspersed between the steep slopes (gully floor and the top of interfluves), which resulted in the steep slopes becoming dissociated from each other and the gully thalweg. Due to the reliance of gHAND on slope to detect wall elements and build on the gully thalweg and floor, badlands are expected to be poorly mapped by gHAND, as was the case in Krumhuk, Namibia.

Lastly, gHAND used proprietary software, eCognition (Trimble, Munich, Bavaria, Germany), to segment the building blocks of gHAND into objects. Although gHAND is built on easily understandable metrics, costs associated with the software may be an obstacle. Nonetheless, we do envisage that gHAND can be implemented at comparable accuracy rates by following a pixel-based approach since the main component is threshold-dependent, which would make the approach more practical for implementation in open-source software such as QGIS (QGIS.org. QGIS Geographic Information System. Open Source Geospatial Foundation Project). There were also some practical limitations to the study itself, as gHAND was tested on an individual gully scale. Further testing should be done on catchment scales when multiple gullies are present. Still, initial indications suggest that accuracy remains unaffected (Olivier et al., 2022), but a practical approach to discriminate gullies from rivers is required. Strategies that can be implemented, some of which have been used in other gully-mapping methodologies, are

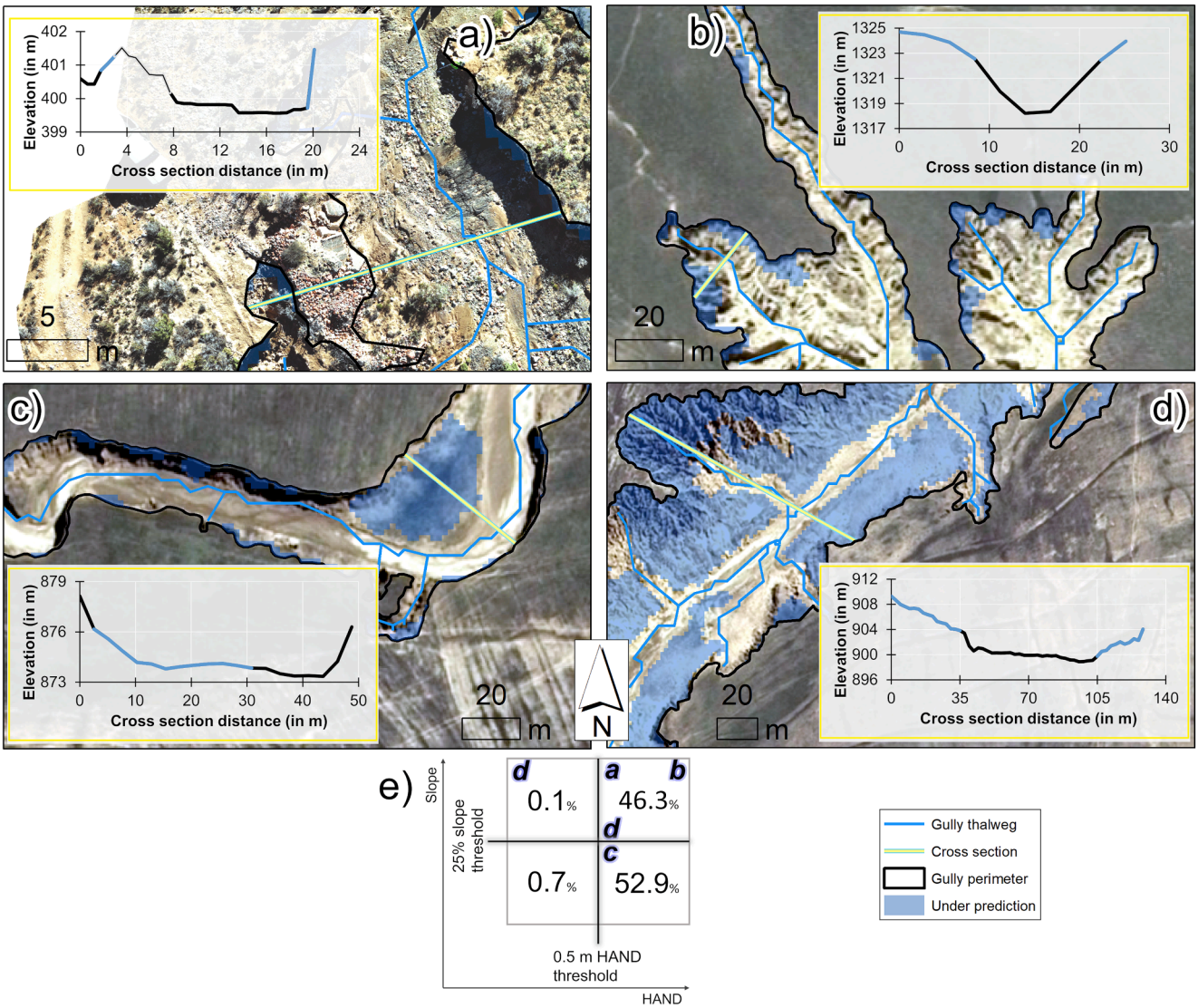

Fig. 11. Areas of under-estimation error by gully HAND symbolised in blue on the aerial imagery and cross sections: a and b) under-estimation pixels in proximity to gully walls with steep slopes and high Height Above Nearest Drainage (HAND) values, c) under-estimation site exhibiting pixels above the low HAND threshold but below the slope threshold, and d) under-estimation area exhibiting pixel values above the slope and below the low HAND thresholds east of the gully thalweg, while above the low HAND threshold on the western gully wall; e) diagram showing in which quadrant the under-estimated pixels are found (n = 188252); the location of the insert maps a, b, c, d are also located in the quadrants. (For interpretation of the references to colour in this figure legend, the reader is referred to the web version of this article.)

applying contributing area thresholds (Castillo et al., 2014; Daba et al., 2003), stream order thresholds (Bartley et al., 2007; Johansen et al., 2012), or using vector overlay from existing river data (Johansen et al., 2012; Olivier et al., 2021). An alternative strategy could also be to implement a discriminatory width-depth ratio.

5.3. Benchmark validation of gHAND

The accuracy of gHAND was comparable with the benchmark workflows at Krumhuk, Namibia and Córdoba, Spain, further validating its transferability.

However, at Krumhuk, the total error incurred by gHAND was 53.2 %. The overall error was strongly associated with under-estimation (47.9 %), which was a result of the gully landform transitioning to a badland. The transition is evident from the historic gully walls being eroded by rill and gully erosion, resulting in the lateral expansion of degraded land, similar to what Boardman et al. (2003) described in the Karoo, SA. Steep gully wall elements are thus lost, which are compounded by the coarse 12 m DEM. The above reasons are likely the cause of the 60.2 % error from the benchmark by Vallejo-Orti et al. (2019), as it also relied on extracting gully elements based on slope characteristics.

The NorToM benchmark (Castillo et al., 2014) was more accurate than gHAND when considering its optimal window size (total error of 10.8 % for NorTom vs 20.8 % for gHAND). The gHAND total error is mainly from over-estimations (17.7 %). The overprediction is likely due to artificial ruggedness from the 0.06 m resolution DEM in proximity to gully walls. The NorToM method would have been able to discriminate better between the artificial ruggedness at the gully wall perimeter due to the application of an additional filter (Castillo et al., 2014 named it UNET) to eliminate areas of high slopes beyond the gully landform.

5.4. Effect of spatial resolution and land use

Like other methodologies, the gHAND workflow depends on the spatial resolution and quality of the derived DEM and to what extent

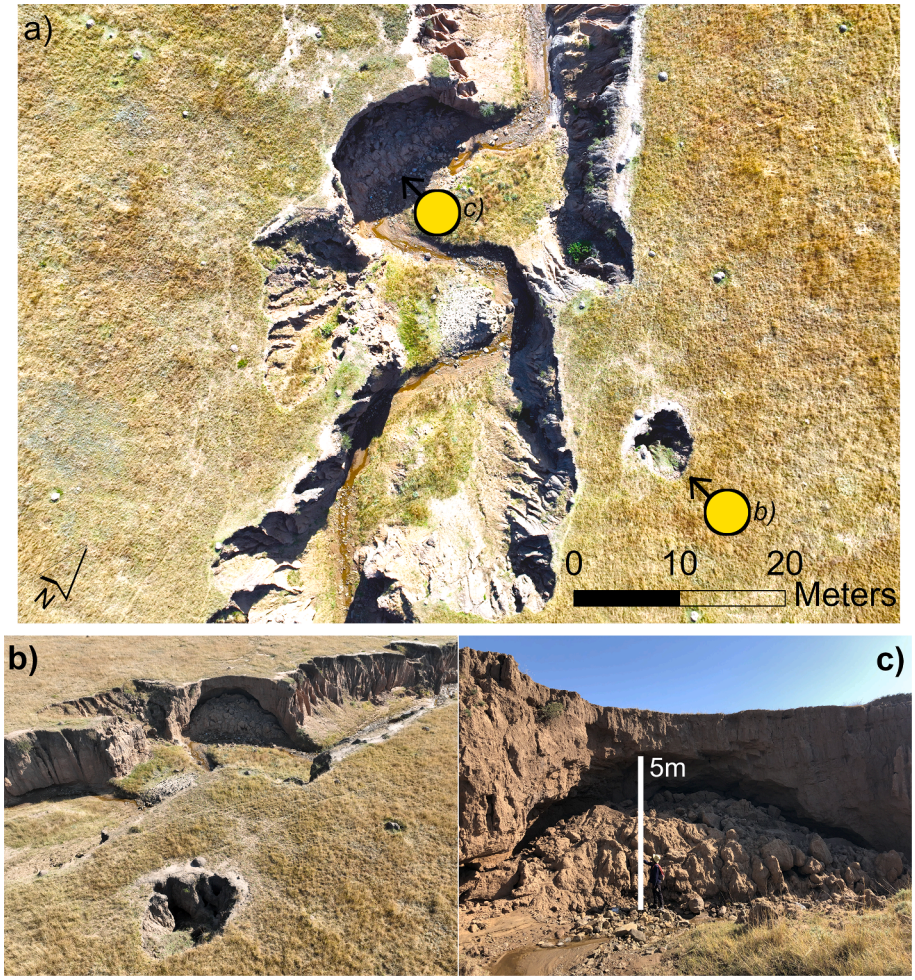

Fig. 12. An extensive gully system in the Tsitsa catchment showing an actively eroding cut bank, with deposition occurring at a point bar: **a)** an aerial photo of the gully taken by a DJI Mavic 3 Unmanned Aerial Vehicle; **b)** the collapse of a large sub-surface pipe is evident in the foreground, which is connected to the gully at a large outlet at the gully wall-floor interface. Significant deposits can be seen at the outer meander wall as well as a shallow low-sloped collapse adjacent to the cut bank (position and direction of photo denoted as b in panel a); **c)** the significant collapse from scour resulting in undercutting of the gully wall at the outer meander gully wall, in addition to grass coverage on the deposited soil at the inner meander bend in the foreground (position and direction of photo denoted as c in panel a).

vegetation coverage (also linked to land use) is captured in the DEM output.

Due to the strong dependence of gHAND on drainage pathways and the identification of short, steep slopes found at gully sidewalls, the DEM spatial resolution impacts performance. Coarsening spatial resolution mostly yielded increases in total errors (Fig. 7; supplementary material, Fig. A3). Higher spatial resolution DEMs can capture more topographical detail, resulting in a better representation of the actual gully morphology, in addition to yielding superior drainage pathway identification (McMaster, 2002). As the spatial resolution coarsens, the under-estimation becomes more prevalent in gHAND output, contrasting with Castillo et al. (2014). The under-estimation of gHAND may be due to the pixel-based shrinking procedure, which was implemented to guard against over-estimation from slopes at the gully walls. However, it could also be due to the coarsening resolution smoothing topography resulting in the reduction or removal of short, steep slope elements (Claessens et al., 2005; Deng et al., 2007), resulting in a loss of gully wall candidates. The latter is evident from increased under-estimation as the DEM resolution coarsens.

The application of gHAND was constrained to areas where fieldwork was conducted in SA and in proximity to areas of application of (semi-) automated methods, thus constraining the application of gHAND to crops, grazing, and conservation land-uses. The areas exhibited limited large vegetation, except for the sites at Herbert, Australia, and Swartland, SA. In Herbert, Australia, a terrain model was derived, thus eliminating vegetation from the DEM used. In Swartland, SA, where vegetation was limited on the crop field but abundant in the gully channel, a total mapping error of 49.8 % occurred. It is, therefore, unlikely that gHAND would adequately map gullies in forested areas, except if a terrain model is derived, such as in Herbert, Australia. Additionally, gHAND may have limitations when applied to urban gullies due to complex hydrological features and proximity of built structures, although further testing would be required to confirm this.

5.5. *Uses of gHAND*

Although gHAND interrogates DEMs using a GEOBIA approach, once set up, it adequately maps gullies in various environments and geomorphic scales. Once the manual mapping of gully headcuts as points are completed, gHAND can rapidly map the full gully extents without the need for editing the workflow. We envisaged its use to aid management strategies as it could be used to identify gully perimeters quickly and, when used temporally, can be used to determine areas of expansion in need of mitigation, in addition to testing the efficacy and lifespans of implemented strategies.

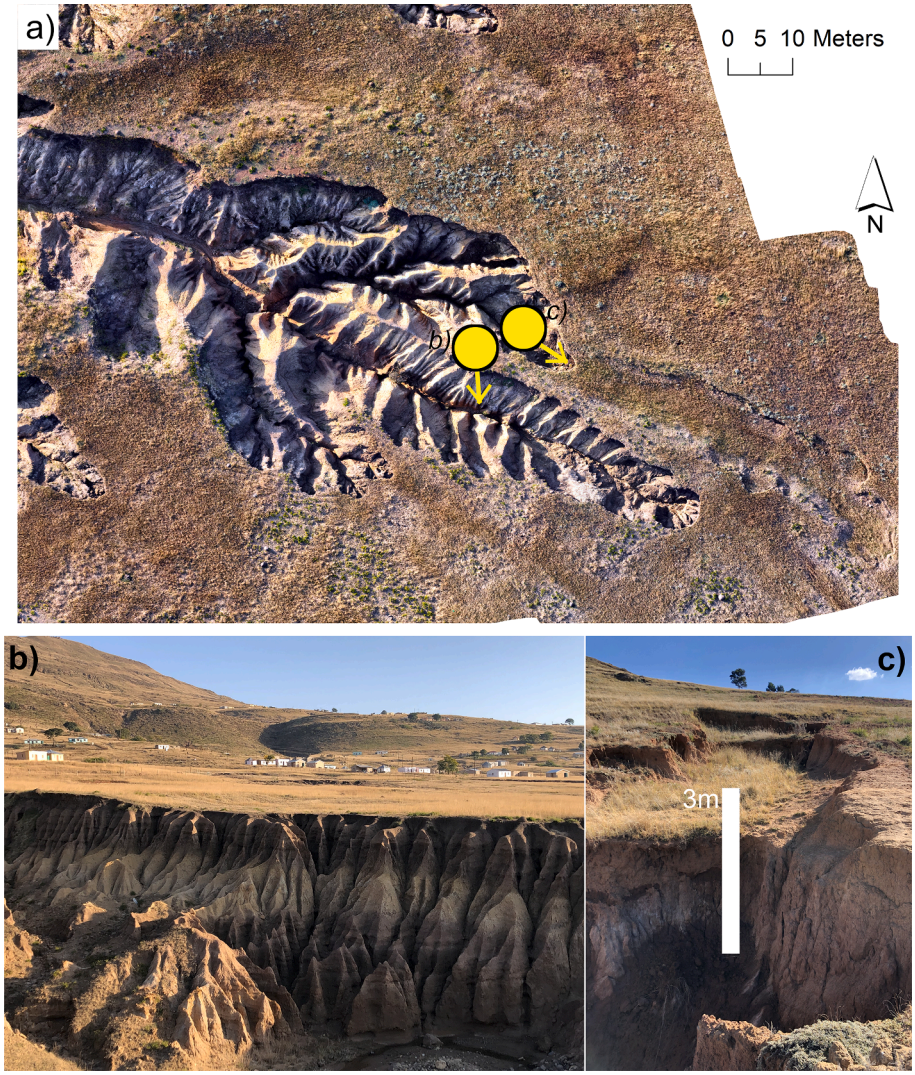

Fig. 13. Typical large complex gully system in the Tsitsa catchment exhibiting steep gully sidewalls, some of which are fluted, and narrow interfluves between gully channel tributaries: **a)** an aerial photo of the gully taken by a DJI Mavic 3 Unmanned Aerial Vehicle; **b)** shows a V-shape channel exhibiting surface flow processes at the gully wall, evident from the fluting sidewalls (position and direction of photo denoted as b in panel a); **c)** an active, near-vertical gully headcut found downstream of a shallow, grass-covered gully channel (position and direction of photo denoted as c in panel a).

6. Conclusion

Herein we developed a new semi-automated gully detection strategy, gHAND, based on geomorphic measurements associated with gully dimensions, which we rigorously tested for scalability and transferability. The gHAND workflow proposed had small differences in accuracy metrics compared with benchmark methods developed for region-specific gully forms. Furthermore, the error rate was similar to previous studies for typical gullies from small- to large-scales. The gHAND workflow shows adaptability to map gullies at contrasting scales and geo-environments, capable of using DEMs derived from different sources with various spatial resolutions. There are limitations associated with the implementation of gHAND, most notably the need to manually digitise gully headcuts. Nevertheless, gHAND shows clear potential for catchment- to regional-scale gully detection. Thus, gHAND can be implemented to map gullies, providing information regarding their location, morphology, and density for various geo-environmental regions. The extracted information can further improve our understanding of how control factors impact gullying on catchment management to regional scales. Because of the ability of the gHAND to extract specific gully features and its unbiased repeatability, we envisage that it can also be used to monitor gullies temporally. For example, gHAND could be implemented to create long-term datasets (>15 years) regarding gully evolution when applied to DEMs retrieved at various temporal intervals, which are still limited in global gully research. These datasets can help identify areas where active gully expansion is concerning or can assist in assessing the efficacy of any mitigation measures.

Conflict of interest

All authors have approved the manuscript and agree with its submission to Catena. The authors declare no conflict of interest. The funders were not involved in the design of the study, the collection, analysis, and interpretation of the compiled data, in writing, reviewing, and editing the manuscript, or in which academic journal to publish.

Funding

This research was partly funded through a Collaborative Research Grant from Coventry University, awarded to Dr. M.J. Van De Wiel and Dr. W.P. de Clercq, and further supported by the National Research Foundation of South Africa through the AUDA-NEPAD SANWATCE WARFSA Aligned Research Grants Programme, awarded to Mr. G. Olivier and Dr. W.P. de Clercq.

Declaration of competing interest

The authors declare the following financial interests/personal relationships which may be considered as potential competing interests: George Olivier reports financial support was provided by AUDA-NEPAD SANWATCE WARFSA. Willem P. de Clercq reports financial support was provided by AUDA-NEPAD SANWATCE WARFSA. George Olivier reports a relationship with AUDA-NEPAD SANWATCE WARFSA that includes: funding grants. Willem P. de Clercq reports a relationship with AUDA-NEPAD SANWATCE WARFSA that includes: funding grants.

Data availability

The gHAND workflow is fully described in the text, therefore repeatable. However, the eCognition Developer 9 workflow file (*.dcp), can be shared upon request. The raw DEM data remains the property of the organisation from where we obtained it, therefore cannot be made available by the corresponding author. The DEM products can however be acquired directly from the organisations, which are referenced in the text.

Acknowledgements

We extend our thanks to the Centre for Geographical Analysis at Stellenbosch University for providing access to spatial datasets in South Africa. We would also like to extend our thanks to Prof. A. van Niekerk who introduced the concept of Height Above Nearest Drainage. This research was supported through the Collaborative Research Grant from Coventry University, awarded to Dr M.J. Van De Wiel and Dr W.P. de Clercq. Further support was received from the National Research Foundation of South Africa through the AUDA-NEPAD SANWATCE WARFSA Aligned Research Grants Programme, awarded to Mr G. Olivier and Dr W.P. de Clercq. The authors would like to thank the reviewers for their constructive comments throughout the review process.

Appendix A. Supplementary material

Supplementary data to this article can be found online at https://doi.org/10.1016/j.catena.2023.107706.

References

Bartley, R., Henderson, A., Prosser, I.P., Hughes, A.O., McKergow, L., Lu, H., Brodie, J., Bainbridge, Z., Roth, C.H., 2003. Patterns of erosion and sediment and nutrient transport in the Herbert River catchment, Queensland. Consultancy Report, CSIRO Land and Water.

Bartley, R., Hawdon, A., Post, D.A., Roth, C.H., 2007. A sediment budget for a grazed semi-arid catchment in the Burdekin basin, Australia. Geomorphology 87 (4), 302–321.

Blaschke, T., Hay, G.J., Kelly, M., Lang, S., Hofmann, P., Addink, E., Feitosa, R.Q., Van der Meer, F., Van der Werff, H., Van Coillie, F., Tiede, D., 2014. Geographic object-based image analysis–towards a new paradigm. ISPRS J. Photogramm. Remote Sens. 87, 180–191.

Boardman, J., Parsons, A.J., Holland, R., Holmes, P.J., Washington, R., 2003. Development of badlands and gullies in the Sneeuberg, Great Karoo, South Africa. Catena 50 (2–4), 165–184.

Bokaei, M., Samadi, M., Hadavand, A., Moslem, A.P., Soufi, M., Bameri, A., Sarvarinezhad, A., 2023. Gully extraction and mapping in Kajoo-Gargaroo watershed-Comparative evaluation of DEM-based and image-based machine learning algorithms. ISPRS Ann. Photogram. Remote Sen. Spat. Inf. Sci. 10, 101–108.

Brecheisen, Z.S., Richter, D.D., 2021. Gully-erosion estimation and terrain reconstruction using analyses of microtopographic roughness and LiDAR. Catena 202, 105264.

Burger, M., 2013. Geology of S. Afr.-1:1,000,000 – chronostratigraphic. Council for Geoscience. http://www.geoscience.org.za/ (Accessed: 1 January 2023).

Castillo, C., Gómez, J.A., 2016. A century of gully erosion research: Urgency, complexity and study approaches. Earth-Sci. Rev. 160, 300–319.

Castillo, C., Taguas, E.V., Zarco-Tejada, P., James, M.R., Gómez, J.A., 2014. The normalized topographic method: an automated procedure for gully mapping using GIS. Earth Surf. Processes Landf. 39 (15), 2002–2015.

Chen, R., Zhou, Y., Wang, Z., Li, Y., Li, F., Yang, F., 2023. Towards accurate mapping of loess gully by integrating google earth imagery and DEM using deep learning. Int. Soil Water Cons. Res.

Claessens, L., Heuvelink, G.B.M., Schoorl, J.M., Veldkamp, A., 2005. DEM resolution effects on shallow landslide hazard and soil redistribution modelling. Earth Surf. Processes and Landf.: The J. of the Br. Geomorphological Res. Group, 30(4), 461-477.

Codru, I.C., Niacsu, L., Enea, A., Bou-imajjane, L., 2023. Gully head-cuts inventory and semi-automatic gully extraction using LiDAR and topographic openness—Case study: Covurlui Plateau, Eastern Romania. Land 12 (6), 1199.

d'Oleire-Oltmanns, S., Marzolff, I., Tiede, D., Blaschke, T., 2014. Detection of gully-affected areas by applying object-based image analysis (OBIA) in the region of Taroudannt, Morocco. Remote Sens. 6 (9), 8287–8309.

Daba, S., Rieger, W., Strauss, P., 2003. Assessment of gully erosion in eastern Ethiopia using photogrammetric techniques. Catena 50 (2–4), 273–291.

Deng, Y., Wilson, J.P., Bauer, B.O., 2007. DEM resolution dependencies of terrain attributes across a landscape. Int. J. Geogr. Inf. Sci. 21 (2), 187–213.

[dataset] Department of Rural Development and Land Reform, 2022. Chief Directorate National Geo-Information portal. http://www.cdngiportal.co.za/cdngiportal/ (Accessed: 20 December 2022).

Evans, M., Lindsay, J., 2010. High resolution quantification of gully erosion in upland peatlands at the landscape scale. Earth Surf. Processes Landf. 35 (8), 876–886.

Fey, M., 2010. Soils of S. Afr.. Cambridge University Press.

Francipane, A., Cipolla, G., Maltese, A., La Loggia, G., Noto, L.V., 2020. Using very high resolution (VHR) imagery within a GEOBIA framework for gully mapping: an application to the Calhoun Critical Zone Observatory. J. Hydroinform. 22 (1), 219–234.

Garousi-Nejad, I., Tarboton, D.G., Aboutalebi, M., Torres-Rua, A.F., 2019. Terrain analysis enhancements to the height above nearest drainage flood inundation mapping method. Water Resour. Res. 55 (10), 7983–8009.

[dataset] Geoscience Australia, 2012. Australian and Region Surface Geology [Online]. Commonwealth of Australia. http://maps.ga.gov.au/interactive-maps/#/theme/minerals/map/geology (Accessed 1 February 2023).

[dataset] GeoSmart Space Pty (Ltd), 2020. 2 m Digital Elevation Model of S. Afr. (DEMSA). https://geosmart.space/products/demsa2.html (Accessed 14 February 2023).

Hayas, A., Poesen, J., Vanwalleghem, T., 2017. Rainfall and vegetation effects on temporal variation of topographic thresholds for gully initiation in Mediterranean cropland and olive groves. Land Degrad. Dev. 28 (8), 2540–2552.

Johansen, K., Taihei, S., Tindall, D., Phinn, S., 2012. Object-based monitoring of gully extent and volume in north Australia using LiDAR data. In: Proceedings of the 4th GEOBIA, p. 25.

Johnson, J.M., Munasinghe, D., Eyelade, D., Cohen, S., 2019. An integrated evaluation of the national water model (NWM)–Height above nearest drainage (HAND) flood mapping methodology. Nat. Haz. Earth Syst. Sci. 19 (11), 2405–2420.

Karydas, C., Jiang, B., 2020. Scale optimization in topographic and hydrographic feature mapping using fractal analysis. ISPRS Int. J. Geo-Inf. 9 (11), 631.

Korzeniowska, K., Pfeifer, N., Landtwing, S., 2018. Mapping gullies, dunes, lava fields, landslides via surface roughness. Geomorphology 301, 53–67.

Laker, M.C., 2004. Advances in soil erosion, soil conservation, land suitability evaluation and land use planning research in South Africa, 1978-2003. S. Afr. J. of Plant and Soil, 21(5), 345-368.

Le Roux, J.J., 2018. Sediment yield potential in South Africa's only large river network without a dam: Implications for water resource management. Land Degrad. Dev. 29 (3), 765–775.

Liu, Y.Y., Maidment, D.R., Tarboton, D.G., Zheng, X., Yildirim, A., Sazib, N.S., Wang, S., 2016. A CyberGIS approach to generating high-resolution height above nearest drainage (HAND) raster for national flood mapping.

Liu, B., Zhang, B., Feng, H., Wu, S., Yang, J., Zou, Y., Siddique, K.H., 2022. Ephemeral gully recognition and accuracy evaluation using deep learning in the hilly and gully region of the Loess Plateau in China. Int. Soil Water Cons. Res. 10 (3), 371–381.

Mararakanye, N., Le Roux, J.J., 2012. Gully location mapping at a national scale for South Africa. S. Afr. Geogr. J. 94, 208–218. https://doi.org/10.1080/03736245.2012.742786.

Mararakanye, N., Nethengwe, N.S., 2012. Gully features extraction using remote sensing techniques. S. Afr. J. Geomatics 1 (2), 109–118.

McMaster, K.J., 2002. Effects of digital elevation model resolution on derived stream network positions. Water Resour. Res. 38 (4), 11–13.

Miguez-Macho, G., Fan, Y., Dominguez, F., 2020, December. Advances in groundwater representation at the subgrid scale in Land Surface Models: an approach based on HAND (height above nearest drainage). In AGU Fall Meeting Abstracts (Vol. 2020, H201-03).

Mucina, L., Rutherford, M.C., 2006. The vegetation of South Africa, Lesotho and Swaziland. Strelitzia 19, (South African National Biodiversity Institute: Pretoria, South Africa). Memoirs of the Botanical Survey of South. Africa.

Nobre, A.D., Cuartas, L.A., Hodnett, M., Rennó, C.D., Rodrigues, G., Silveira, A., Saleska, S., 2011. Height above the nearest drainage–A hydrologically relevant new terrain model. J. Hydrol. 404 (1–2), 13–29.

O'Callaghan, J.F., Mark, D.M., 1984. The extraction of drainage networks from digital elevation data. Comput. Vis. Graph. Image Process. 28 (3), 323–344.

Olivier, G., van de Wiel, M., de Clercq, W., 2021, April. Semi-automated detection of gully slivers from a Digital Surface Model in rough agricultural terrain. In EGU General Assembly Conference Abstracts (EGU21-5747).

Olivier, G., Van De Wiel, M., De Clercq, W., 2022. Giving gully detection a HAND (No. ICG2022-102). Copernicus Meetings.

Osumgborogwu, I.E., Wainwright, J., Turnbull, L., Uzoigwe, L.O., 2022. A multi-method approach to analyse changes in gully characteristics between 2009 and 2018 in southeast Nigeria. Land Degrad. Dev. 33 (9), 1398–1409.

Perroy, R.L., Bookhagen, B., Asner, G.P., Chadwick, O.A., 2010. Comparison of gully erosion estimates using airborne and ground-based LiDAR on Santa Cruz Island, California. Geomorphology 118 (3–4), 288–300.
Phinzi, K., Abriha, D., Szabó, S., 2021. Classification efficacy using k-fold cross-validation and bootstrapping resampling techniques on the example of mapping complex gully systems. Remote Sens. 13 (15), 2980.
Phinzi, K., Abriha, D., Bertalan, L., Holb, I., Szabó, S., 2020. Machine learning for gully feature extraction based on a pan-sharpened multispectral image: Multiclass vs. Binary approach. ISPRS Int. J. of Geo-Inf., 9(4), 252.
Planchon, O., Darboux, F., 2002. A fast, simple and versatile algorithm to fill the depressions of digital elevation models. Catena 46 (2), 159–176.
Poesen, J., Nachtergaele, J., Verstraeten, G., Valentin, C., 2003. Gully erosion and environmental change: importance and research needs. Catena 50 (2–4), 91–133.
Rennó, C.D., Nobre, A.D., Cuartas, L.A., Soares, J.V., Hodnett, M.G., Tomasella, J., 2008. HAND, a new terrain descriptor using SRTM-DEM: Mapping terra-firme rainforest environments in Amazonia. Remote Sens. Environ. 112 (9), 3469–3481.
Rijal, S., Wang, G., Woodford, P.B., Howard, H.R., Hutchinson, J.S., Hutchinson, S., Schoof, J., Oyana, T.J., Li, R., Park, L.O., 2018. Detection of gullies in Fort Riley military installation using LiDAR derived high resolution DEM. J. Terramech. 77, 15–22.
Rossi, M., Torri, D., De Geeter, S., Cremer, C., Poesen, J., 2022. Topographic thresholds for gully head formation in badlands. Earth Surf. Processes Landf. 47 (15), 3558–3587.
Schulze RE, Lynch SD, Maharaj M. (2006) Annual Precipitation, in: Schulze R.E. (Ed.), South African Atlas of Climatology and Agrohydrology. Water Research Commission, Pretoria, RSA, WRC Report 1489/1/06, Section 6.2.
Shellberg, J.G., Brooks, A., 2012. Alluvial gully erosion: A dominant erosion process across tropical Northern Australia. Charles Darwin University.
Shruthi, R.B., Kerle, N., Jetten, V., 2011. Object-based gully feature extraction using high spatial resolution imagery. Geomorphology 134 (3–4), 260–268.
Taruvinga K. 2008. Gully mapping using remote sensing: Case study in KwaZulu-Natal, South Africa. MSc., University of Waterloo.
Thwaites, R.N., Brooks, A.P., Pietsch, T.J., Spencer, J.R., 2022. What type of gully is that? The need for a classification of gullies. Earth Surf. Processes Landf. 47 (1), 109–128.
Torri, D., Poesen, J., 2014. A review of topographic threshold conditions for gully head development in different environments. Earth Sci. Rev. 130, 73–85.
Trimble Germany GmbH, 2023. Trimble Documentation eCognition Developer 9 User Guide; Trimble Germany GmbH: Munich, Germany.
Utsumi, A.G., Pissarra, T.C.T., Rosalen, D.L., Martins Filho, M.V., Rotta, L.H.S., 2020. Gully mapping using geographic object-based image analysis: A case study at catchment scale in the Brazilian Cerrado. Remote Sens. Appl.: Soc. Environ. 20, 100399.
Vallejo-Orti, M., Negussie, K., Corral-Pazos-de-Provens, E., Höfle, B., Bubenzer, O., 2019. Comparison of three algorithms for the evaluation of TanDEM-X data for gully detection in krumhuk farm (Namibia). Remote Sens. 11 (11), 1327.
Vandekerckhove, L., Poesen, J., Wijdenes, D.O., De Figueiredo, T., 1998. Topographical thresholds for ephemeral gully initiation in intensively cultivated areas of the Mediterranean. Catena 33 (3–4), 271–292.
Vanmaercke, M., Panagos, P., Vanwalleghem, T., Hayas, A., Foerster, S., Borrelli, P., Rossi, M., Torri, D., Casali, J., Borselli, L., Vigiak, O., 2021. Measuring, modelling and managing gully erosion at large scales: A state of the art. Earth-Sci. Rev. 218, 103637.
Vrieling, A., Rodrigues, S.C., Bartholomeus, H., Sterk, G., 2007. Automatic identification of erosion gullies with ASTER imagery in the Brazilian Cerrados. Int. J. Remote Sens. 28 (12), 2723–2738.
Walker, S.J., Wilkinson, S.N., van Dijk, A.I., Hairsine, P.B., 2020. A multi-resolution method to map and identify locations of future gully and channel incision. Geomorphology 358, 107115.
Wen, Y., Kasielke, T., Li, H., Zepp, H., Zhang, B., 2021. A case-study on history and rates of gully erosion in Northeast China. Land Degrad. Dev. 32 (15), 4254–4266.
Wilkinson, S.N., Bartley, R., Hairsine, P.B., Bui, E.N., Gregory, L., Henderson, A.E., 2015. Managing gully erosion as an efficient approach to improving water quality in the Great Barrier Reef lagoon. Report to the Department of the Environment.